

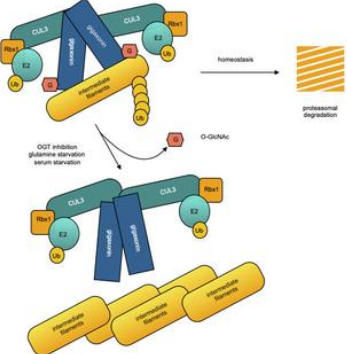
Gigaxonin glycosylation regulates intermediate filament turnover and may impact giant axonal neuropathy etiology or treatment

Po-Han Chen, ... , Jen-Tsan Chi, Michael Boyce

JCI Insight. 2019. <https://doi.org/10.1172/jci.insight.127751>.

Research In-Press Preview Cell biology

Graphical abstract



Find the latest version:

<https://jci.me/127751/pdf>



1 Gigaxonin glycosylation regulates intermediate filament turnover and may impact
2 giant axonal neuropathy etiology or treatment
3 Po-Han Chen^{1,2,3}, Jimin Hu¹, Jianli Wu^{2,3}, Duc T. Huynh¹, Timothy J. Smith¹, Samuel
4 Pan^{2,3}, Brittany J. Bisnett¹, Alexander B. Smith^{2,3}, Annie Lu^{2,3}, Brett M. Condon¹, Jen-
5 Tsan Chi^{2,3,*} and Michael Boyce^{1,*}

6

7 ¹Department of Biochemistry, ²Department of Molecular Genetics and Microbiology
8 and ³Center for Genomic and Computational Biology, Duke University School of
9 Medicine, Durham, NC 27710, U.S.A.

10 *Co-Correspondence: michael.boyce@duke.edu and jentsan.chi@duke.edu

11 Mailing address: 101 Science Drive, 2177A CIEMAS, Box 3382 Durham, NC 27708
12 (JTC); Box 3711 DUMC, Durham, NC 27710 (MB)

13 Phone: 919-668-4759 (JTC); 919-684-9906 (MB)

14

15 Conflict of interest: The authors have declared that no conflict of interest exists.

16

17

18

19

20

21

22

23

24

25 **Abstract**

26

27 Gigaxonin (also known as KLHL16) is an E3 ligase adaptor protein that promotes the
28 ubiquitination and degradation of intermediate filament (IF) proteins. Mutations in
29 human gigaxonin cause the fatal neurodegenerative disease giant axonal neuropathy
30 (GAN), in which IF proteins accumulate and aggregate in axons throughout the nervous
31 system, impairing neuronal function and viability. Despite this pathophysiological
32 significance, the upstream regulation and downstream effects of normal and aberrant
33 gigaxonin function remain incompletely understood. Here, we report that gigaxonin is
34 modified by O-linked β -N-acetylglucosamine (O-GlcNAc), a prevalent form of
35 intracellular glycosylation, in a nutrient- and growth factor-dependent manner. Mass
36 spectrometry analyses of human gigaxonin revealed nine candidate sites of O-
37 GlcNAcylation, two of which – serine 272 and threonine 277 – are required for its
38 ability to mediate IF turnover in novel gigaxonin-deficient human cell models that we
39 created. Taken together, these results suggest that nutrient-responsive gigaxonin O-
40 GlcNAcylation forms a regulatory link between metabolism and IF proteostasis. Our
41 work may have significant implications for understanding the non-genetic modifiers of
42 GAN phenotypes and for the optimization of gene therapy for this disease.

43

44

45

46

47

48 **Introduction**

49

50 *Giant axonal neuropathy (GAN)*

51 Giant axonal neuropathy (GAN) is a rare neurodegenerative disease
52 characterized by abnormally large and dysfunctional axons (1). GAN first manifests as
53 severe peripheral motor and sensory neuropathy during infancy and later evolves into
54 central nervous system pathology, including seizures and cognitive impairment (2-4).
55 Most individuals afflicted with GAN become non-ambulatory early in the first decade
56 of life and eventually develop widespread polyneuropathy and dementia (1, 5). Death
57 usually occurs from respiratory failure by age 40 (1, 5).

58 GAN is caused by loss-of-function mutations in the *GAN* gene, which encodes
59 the gigaxonin protein (2). Gigaxonin (also known as KLHL16) belongs to the Kelch-
60 like (KLHL) protein family, which typically contains Broad complex/Tramtrack/Bric-
61 à-bric (BTB), BTB and C-terminal Kelch (BACK), and Kelch domains (6). Structural
62 and functional studies in representative KLHL family members have demonstrated that
63 the BTB domain interacts with cullin 3 (CUL3), a component of E3 ubiquitin ligase
64 complexes, while the KLHL Kelch domains recruit substrates for polyubiquitination
65 (7). Therefore, KLHL proteins are generally considered to be adaptors for CUL3-
66 containing E3 ligase complexes, regulating the ubiquitination and, usually, proteolysis
67 of specific substrates.

68 Gigaxonin promotes the ubiquitination and turnover of IFs, and defective
69 gigaxonin in GAN patients causes neurofilament-L (NF-L) and other IF proteins to
70 accumulate in the axons of neurons (2, 8, 9). Interestingly, this function of gigaxonin is
71 not restricted to the nervous system. For example, gigaxonin is required for the normal
72 proteolysis of vimentin and keratins in fibroblasts, and GAN patients often exhibit curly

73 hair due to high keratin levels (10, 11). Disease-causing *GAN* mutations disable
74 gigaxonin by several mechanisms, including reducing the abundance of its mRNA,
75 destabilizing the protein and/or impairing its biochemical activity (9). Reciprocally,
76 experimental re-expression of gigaxonin in wild type (WT) or *GAN*-deficient cells
77 results in the clearance of accumulated IFs (12).

78 While the regulation and function of gigaxonin remain incompletely understood,
79 several lines of evidence suggest possible connections to cell metabolism. For example,
80 *GAN*-deficient cells exhibit dysregulated mitochondrial distribution and behavior (10,
81 13). In *GAN* loss-of-function cells, mitochondria often co-localize with ovoid IF
82 aggregates, frequently found near the nucleus, and mitochondrial motility is reduced
83 (10, 13). Although mitochondrial inner membrane potential is not affected by loss of
84 gigaxonin function (13), the oxygen consumption rate is increased in *GAN* knockout,
85 *GAN* knockdown and *CUL3* knockdown cells (10), consistent with functional links
86 among gigaxonin/CUL3 complexes, IFs and mitochondrial physiology. Furthermore,
87 while ovoid IF aggregates are observed in 3 to 15% of *GAN*-deficient cells grown under
88 standard culture conditions, this phenotype is significantly exacerbated (to 48 to 88%)
89 by serum starvation (8), indicating that nutrient or growth factor signaling impacts
90 gigaxonin function. Therefore, the severity of *GAN* phenotypes may be modulated by
91 such non-genetic factors as metabolic status. Together, these observations suggest that
92 nutrient cues affect the activity of gigaxonin and its regulation of the IF cytoskeleton,
93 but the underlying mechanisms remain unknown.

94

95 *O-GlcNAcylation and the KLHL family*

96 In previous work, we discovered a novel connection between the KLHL protein
97 family and O-GlcNAcylation (14). O-GlcNAc is an abundant form of intracellular

98 glycosylation that reversibly decorates serines and threonines of thousands of nuclear,
99 cytoplasmic and mitochondrial proteins (15, 16). In mammals, O-GlcNAc is added by
100 O-GlcNAc transferase (OGT) and removed by O-GlcNAcase (OGA) in response to a
101 wide range of physiological signals (15-18). UDP-GlcNAc, the nucleotide-sugar cofactor
102 used by OGT, is created by the hexosamine biosynthetic pathway (HBP) from multiple
103 essential metabolites, including glucose, glutamine, acetyl-coenzyme A, uridine and ATP
104 (19-22). Therefore, fluctuations in these nutrients or growth factors affect the levels of
105 both UDP-GlcNAc and O-GlcNAc, making the modification a sentinel of cell
106 metabolism (16, 22-30). O-GlcNAc cycling controls myriad processes, including cell
107 metabolism, cell cycle progression and cell death (15, 16, 18) and is essential, as genetic
108 ablation of OGT or OGA in mice is lethal (31-33). Aberrant O-GlcNAcylation is also
109 implicated in numerous human diseases, including various forms of neurodegeneration,
110 further underscoring its functional importance (22, 34-42).

111 Recently, we reported that the KLHL family member KEAP1 (also known as
112 KLHL19) is O-GlcNAcylated. Specific O-GlcNAc sites are necessary for the ability of
113 KEAP1 to mediate the ubiquitination and destruction of NRF2, its best-known target
114 and a master transcriptional regulator of redox stress responses (14, 43, 44). Due to the
115 structural and functional similarities among the KLHL proteins, we speculated that
116 other family members may also be O-GlcNAcylated. Indeed, a pilot experiment
117 suggested that gigaxonin is a potential O-GlcNAc substrate (14). Here, we report that
118 gigaxonin is O-GlcNAcylated on up to nine specific residues in a nutrient-responsive
119 manner. Using novel human gigaxonin loss-of-function neuroblastoma and fibroblast
120 model systems that we created, we identified two specific gigaxonin O-GlcNAc sites
121 that are required for its ability to interact with IF proteins and to promote their turnover.
122 Our results provide new molecular insight into the potential metabolic regulation of the

123 IF cytoskeleton through gigaxonin O-GlcNAcylation and may inform our
124 understanding of GAN disease modifiers and the optimization of GAN gene therapy.

125

126 **Results**

127

128 *Mass spectrometry identifies candidate O-GlcNAc sites on gigaxonin*

129 In a previous study focused on KEAP1 glycosylation (14), we discovered initial
130 evidence of gigaxonin modification by O-GlcNAc. We hypothesized that gigaxonin O-
131 GlcNAcylation might regulate its function in IF protein turnover, analogous to the role
132 of KEAP1 O-GlcNAcylation in governing the ubiquitination and stabilization of its
133 target NRF2 (14). To test this hypothesis, we first confirmed the O-GlcNAcylation of
134 endogenous gigaxonin in a variety of cell types. In SH-SY5Y neuroblastoma cells,
135 gigaxonin is dynamically O-GlcNAc-modified, as the degree of glycosylation was
136 reduced by treatment with a small molecule inhibitor of OGT (Ac4SGlcNAc, or 5SG)
137 and enhanced by a small molecule inhibitor of OGA (Thiamet-G) (Figure 1A). Because
138 gigaxonin regulates IF proteins in non-neuronal tissues as well (45-47), we asked
139 whether these observations extended to other cell types. Indeed, we observed dynamic
140 gigaxonin O-GlcNAcylation in both HeLa (Figure 1B) and MDA-MB-231 cells (Figure
141 1C), supporting gigaxonin O-GlcNAcylation as a broad phenomenon across disparate
142 cell types.

143 To identify O-GlcNAcylated residues on gigaxonin, we expressed myc-6xHis-
144 tagged gigaxonin (MH-gigaxonin) in 293T cells, a facile human expression system, and
145 obtained highly purified protein via tandem IP using anti-myc antibody and
146 immobilized metal affinity chromatography (Figure 1D). Purified gigaxonin from two
147 biological replicates was digested in-gel and analyzed by mass spectrometry (MS) to

148 identify O-GlcNAc sites.

149 In our first MS experiment, we identified nine candidate O-GlcNAc sites on
150 gigaxonin. Five sites (T207, S219, S224, S228 and S229) reside in the BACK domain,
151 which was recently reported to be required for interaction with the autophagy protein
152 ATG16L1 (48). Three other sites (S249, S254, S272) lie in the junction between the
153 BACK and the first Kelch domains and the last site (T277) is within the first Kelch
154 domain, which was predicted to interact with gigaxonin's ubiquitination substrates (49)
155 (Figure 1E and S1A). In a second MS analysis of an independently expressed and
156 purified gigaxonin sample, we again observed the glycosylation of S228, S229, S272
157 and T277, underlining the reproducibility of the methodology and providing strong
158 evidence for the O-GlcNAcylation of these residues.

159 To identify the major *in vivo* O-GlcNAcylation site(s) on gigaxonin, we
160 expressed WT or unglycosylatable (Ser/Thr→Ala) point-mutant constructs in 293T
161 cells and analyzed them by IP/WB. No single point mutation dramatically reduced total
162 detectable gigaxonin O-GlcNAcylation under standard culture conditions, possibly due
163 to the simultaneous modification of multiple sites or to technical limitations of the
164 available anti-O-GlcNAc antibodies (data not shown). On the other hand, upon
165 inhibition of OGA by Thiamet-G, the S272A and T277A mutants, when compared to
166 WT, showed modestly impaired increases in O-GlcNAc signal (Figure S1B). This result
167 suggests that inducible gigaxonin O-GlcNAcylation may occur primarily at S272
168 and/or T277.

169

170 *Gigaxonin loss-of-function neuroblastoma and fibroblast cells provide novel GAN*
171 *model systems*

172 Primary fibroblasts from GAN patients have been powerful tools for dissecting

173 the functional impact of gigaxonin mutants, but they are genetically heterogeneous and
174 often exhibit variable IF phenotypes (e.g., 3 to 15% of cells displaying ovoid
175 aggregates), which may confound the interpretation of some experiments (8, 50).
176 Mouse models of GAN have also been valuable but exhibit less severe
177 neurodegeneration than do human patients, suggesting potentially important species-
178 dependent differences (51-53). Therefore, we sought to use CRISPR genome
179 engineering to ablate endogenous gigaxonin expression in human cells, establishing
180 *GAN*^{-/-} systems that reliably recapitulate cellular GAN disease phenotypes and permit
181 functional tests of gigaxonin mutants. We envision that such tractable human cell lines
182 would provide a useful complement to existing GAN primary cell and mouse systems.
183 We chose SH-SY5Y and BJ5ta (immortalized human fibroblast) cells as appropriate
184 models, based on previous reports of gigaxonin function and IF protein accumulation
185 in these cell types (12). Multiple guide RNAs (gRNA) targeting *GAN* exon 1 were
186 designed and sub-cloned into a lentiCRISPR vector (54). After selection, *GAN*^{-/-} SH-
187 SY5Y cells exhibited reduced proliferation and often grew as individual cells instead
188 of the clusters seen in the parental cell line (Figure S2A).

189 To confirm successful *GAN* deletion, we evaluated gigaxonin and vimentin
190 expression in *GAN*^{-/-} cells by WB and qPCR. Gigaxonin protein and mRNA were
191 depleted in the *GAN*-targeted cells (Figure 2A and B), with a corresponding dramatic
192 increase in endogenous vimentin protein (Figure 2A and S2B). By immunofluorescence
193 assay (IFA), most *GAN*^{-/-} SH-SY5Y (Figure 2C) and BJ5ta (Figure S2C) cells showed
194 single, perinuclear and ovoid-shaped vimentin aggregates, similar to previously
195 reported phenotypes in primary cells from GAN patients (Figure 2C) (8, 12).
196 Quantification of distinct *GAN*^{-/-} cell lines generated with different sgRNA showed that
197 >80% of cells (in sgRNAs 1 and 3) contained perinuclear ovoid aggregates. Aggregates

198 co-localized with the microtubule organizing center but not with Golgi markers (Figure
199 2E-F). Consistent with a previous report (8), F-actin distribution was not affected by
200 gigaxonin loss (Figure 2G), demonstrating the specific effect of *GAN* deletion on the
201 IF compartment. In addition, we also observed aggregation and co-localization of NF-
202 L with vimentin in *GAN*^{-/-} SH-SY5Y cells (Figure 2H).

203 To further confirm our CRISPR results by an independent method, we
204 established stable shRNA-mediated *GAN* knockdown cell lines (shGAN). As expected,
205 we observed vimentin increases and aggregation in shGAN SH-SY5Y cells using both
206 WB (Figure S2D) and IFA (Figure S2E). Importantly, shGAN cells showed similar
207 cellular morphology as *GAN*^{-/-} cells, and re-expression of WT shRNA-resistant
208 gigaxonin (V5-GAN^R; R: shRNA-resistant) abolished both the vimentin accumulation
209 (Figure S2D, E, and F) and the cellular morphology phenotypes (Figure S2G). Rescue
210 of these GAN-like phenotypes by gigaxonin re-expression confirms the specificity and
211 validity of our cell systems.

212 Taken together, these results show that engineered *GAN*-deficient
213 neuroblastoma and fibroblast cell lines phenocopy pathophysiologically relevant
214 characteristics of GAN patient cells (8), indicating that they are tractable and
215 appropriate models for evaluating the function of gigaxonin O-GlcNAcylation.

216

217 *S272 and T277 O-GlcNAc sites are required for gigaxonin function*

218 To evaluate the functional significance of the gigaxonin O-GlcNAc sites we
219 identified, we harnessed the disease-relevant vimentin aggregation phenotype of *GAN*^{-/-}
220 cells (Figure 2) to assess the function of unglycosylatable gigaxonin point-mutants.
221 First, we expressed HA-tagged WT or S52G mutant gigaxonin (a known loss-of-
222 function GAN disease allele, as a control (12)) in *GAN*^{-/-} SH-SY5Y cells and performed

223 IFA. As shown previously, *GAN*^{-/-} SH-SY5Y cells exhibited dramatically increased
224 vimentin levels, compared to controls (Figure 3A, upper two rows). Re-expression of
225 WT gigaxonin (HA-WT-gigaxonin) markedly repressed vimentin levels (Figure 3A,
226 3rd to 5th rows; Figure S3A), whereas the disease-causing S52G mutant did not (Figure
227 3A, 6th row; Figure S3A) (12). These results confirm that the vimentin aggregation
228 phenotype of *GAN*^{-/-} cells is an appropriate assay for assessing the function of WT and
229 mutant gigaxonin.

230 Next, we used *GAN*^{-/-} cells to test the function of the nine unglycosylatable
231 gigaxonin point-mutants. Interestingly, among all mutants, only S272A and T277A
232 consistently failed to clear or prevent the formation of ovoid bundles, exhibiting a
233 partial loss-of-function phenotype across three independent experiments (Figure 3B
234 and S3B). We recently reported that vimentin O-GlcNAcylation regulates IF structure
235 and function (55). Therefore, we investigated whether vimentin glycosylation could
236 impact its turnover by WT or mutant gigaxonin as well. We found that WT gigaxonin
237 expression reduced WT vimentin levels more efficiently than S272A or T277A
238 gigaxonin did in EGFP-WT-vimentin reconstituted Vimentin^{-/-} HeLa cells (55) (Figure
239 3C and D). In contrast, the unglycosylatable S49A vimentin mutant, which lacks O-
240 GlcNAc at a crucial site (55), is a poorer substrate for WT, S272A and T277A gigaxonin
241 alike, as compared to WT vimentin (Figures S3C and S3D). These results indicate that
242 O-GlcNAcylation of gigaxonin substrates may also affect their proteasome-mediated
243 degradation. Therefore, O-GlcNAc signaling may impact the proteostasis of IFs in
244 several ways, an important subject for future studies. With respect to gigaxonin in
245 particular, these data indicate that the S272 and T277 O-GlcNAcylation sites are critical
246 for its ability to regulate IF protein levels. Given that S272 and T277 may also be the
247 primary sites of inducible gigaxonin O-GlcNAcylation (Figure S1), the dynamic, site-

248 specific glycosylation of S272 and T277 may be required for normal gigaxonin activity
249 in cells.

250 Because gigaxonin and CUL3 interact genetically and biochemically, we
251 hypothesized that loss of gigaxonin O-GlcNAcylation at specific sites might affect
252 these functional interactions, analogous to our prior results with KEAP1 (14). To test
253 this possibility, we co-expressed WT or unglycosylatable gigaxonin mutants with
254 CUL3 in 293T cells and examined their effects on endogenous IF proteins. 293T cells
255 transfect efficiently, express endogenous vimentin and NF, and have served as a
256 tractable and useful model for studying the molecular mechanism of gigaxonin
257 previously, making them an appropriate system for these experiments (12, 49, 56).
258 Overexpression of gigaxonin significantly reduces vimentin levels even in cells that
259 express endogenous gigaxonin (12). CUL3 overexpression alone had no effect on
260 vimentin but co-expression of CUL3 and gigaxonin further reduced vimentin levels, as
261 predicted by their established functional interaction (Figure S4A). In contrast, co-
262 expression of the S52G gigaxonin mutant with CUL3 failed to reduce vimentin and NF-
263 L levels, compared to WT gigaxonin (Figure 4A), in agreement with a previous report
264 (12). Consistent with our results in *GAN*^{-/-} cells (Figure 3), co-expression of the S272A
265 or T277A mutant with CUL3 failed to reduce vimentin and NF-L levels (Figure 4A and
266 B). Collectively, these data highlight the importance of the S272 and T277 gigaxonin
267 O-GlcNAcylation sites in governing the degradation of IF proteins.

268

269 *Gigaxonin O-GlcNAcylation sites are required for interaction with IF proteins*

270 Gigaxonin is thought to be an adaptor for CUL3-containing E3 ligase
271 complexes, mediating the ubiquitination and degradation of IF proteins. Gigaxonin
272 interacts with both CUL3 (7) and the E1 through its BTB domain (57). Truncation

273 mutants and biochemical experiments have demonstrated that the gigaxonin Kelch
274 domains interact with ubiquitination targets, such as tubulin cofactor B (58, 59) and
275 vimentin (49). However, the specific residues on gigaxonin critical for interacting with
276 these targets remain unidentified.

277 Based on our prior studies of KEAP1 glycosylation (14), we hypothesized that O-
278 GlcNAcylation of gigaxonin might influence its biochemical interactions with CUL3
279 or with IF proteins themselves. In support of this idea, STRING analysis, based on
280 direct and indirect interactome databases (60), suggested that gigaxonin interacts with
281 several E3 ligase components, including CUL3 and ring box protein1 (RBX1) (Figure
282 S4B) (61). We experimentally reconfirmed the biochemical interaction between
283 endogenous CUL3 and gigaxonin via co-IP and WB (Figure S4C). Interestingly, the
284 CUL3/gigaxonin interaction was not affected by the S272A or T277A mutations (Figure
285 5A, lanes 7 and 8), likely because these residues lie outside the BTB domain thought to
286 interact with CUL3 (7).

287 Next, we tested whether the interactions between gigaxonin and its substrates
288 vimentin or NF-L were affected by O-GlcNAc site mutations. The molecular weight of
289 endogenous vimentin (54 kDa) is close to IgG heavy chain, which would complicate
290 the interpretation of IP/WB results. Therefore, we used a previously validated EGFP-
291 vimentin construct (55) for these experiments. EGFP-vimentin and HA-gigaxonin
292 constructs (WT, S272A or T277A mutants) were co-transfected into 293T cells. Co-IP
293 assays confirmed a robust interaction between WT gigaxonin and EGFP-vimentin, as
294 expected (Figure 5B) (55, 62). However, the interaction between vimentin and S272A
295 or T277A gigaxonin, as compared to WT, was consistently reduced when IP-ed by
296 either HA (gigaxonin) or GFP (vimentin) antibodies (Figure 5B, lanes 7 vs. 8 or 11 vs.
297 12). A similarly reduced interaction was also observed between soluble endogenous

298 NF-L and expressed S272A or T277A gigaxonin, compared to WT (Figure 5B, lane 7
299 and 8, C and D). Moreover, the S272A and T277A gigaxonin mutants triggered less
300 polyubiquitination of vimentin, compared to WT (Figure 5E), indicating a functional
301 impact of this reduced biochemical interaction. Together, these data demonstrate that
302 the S272 and T277 gigaxonin glycosylation sites are critical for its optimal interaction
303 with IF proteins, leading to polyubiquitination and protein turnover.

304

305 *The effects of nutrients and GAN-associated mutations on gigaxonin O-GlcNAcylation*

306 Because O-GlcNAc is a nutrient-sensitive modification (18, 63, 64), we
307 hypothesized that various metabolic conditions might affect gigaxonin O-
308 GlcNAcylation, similar to our prior results with KEAP1 (43, 44). In support of this
309 possibility, Bomont and Koenig showed that the vimentin aggregation observed in *GAN*
310 loss-of-function cells was aggravated by serum starvation or microtubule
311 depolymerization (8), treatments also known to induce global O-GlcNAc changes (59,
312 65-67). Therefore, we tested whether gigaxonin O-GlcNAcylation is impacted by
313 serum starvation. Interestingly, IP/WB experiments revealed that serum starvation
314 consistently reduced gigaxonin glycosylation, as judged by two different anti-O-
315 GlcNAc monoclonal antibodies (Figure 6A, lane 4 vs. 5). In the same samples, we also
316 observed the accumulation of vimentin under serum starvation (Figure S5), reminiscent
317 of the enhanced vimentin aggregation when *GAN* patient fibroblasts were similarly
318 treated (8). In another independent test of our hypothesis, gigaxonin O-GlcNAcylation
319 was reduced by deprivation of glucose and glutamine (68), essential nutrients feeding
320 the HBP (Figure 6B, lane 5 vs. 6 and 6C). From these results, we concluded that
321 gigaxonin O-GlcNAcylation is responsive to nutrient levels.

322

323 **Discussion**

324

325 Here we report that the KLHL protein gigaxonin is O-GlcNAcylated in a
326 nutrient- and serum-responsive manner. Of nine candidate O-GlcNAc sites we
327 identified, S272 and T277 are glycosylated and required for gigaxonin's full interaction
328 with, and ubiquitination of, IF proteins. Our new loss-of-function *GAN* models display
329 classical ovoid vimentin aggregates in a consistent and robust manner, enabling genetic
330 complementation experiments to measure the impact of individual point-mutations on
331 IF protein turnover. These experiments further confirmed the functional significance of
332 the S272 and T277 O-GlcNAc sites. Together, our results suggest that stimulus-induced
333 O-GlcNAcylation of gigaxonin may be required for its optimal ability to regulate IF
334 protein turnover, perhaps by inducing a conformational change in gigaxonin that
335 promotes IF protein binding (Figure 7).

336

337 *New culture models of GAN*

338 Current models for GAN rely primarily on patient-derived fibroblasts (8, 12,
339 50), induced pluripotent stem cells (69) or *GAN*^{-/-} mice (13, 51-53). Though valuable,
340 patient-derived cells have heterogeneous genetic backgrounds and display incompletely
341 penetrant IF phenotypes (e.g., 3 to 15% of cells displaying ovoid aggregates), which
342 may complicate the interpretation of mechanistic and functional studies. *GAN*^{-/-} mice
343 have also been powerful systems but do not fully phenocopy human GAN symptoms,
344 suggesting important species-dependent differences (13, 51-53). Using CRISPR-
345 mediated gene deletion, we developed *GAN*^{-/-} models in both GAN-relevant human
346 fibroblast and neuroblastoma cell lines (12), in which more than 80% of *GAN*^{-/-} cells

347 display ovoid-shaped vimentin aggregates (Figure 2). These human *GAN*^{-/-} cell lines are
348 easier to propagate and manipulate experimentally than are patient-derived cells or mice
349 and will therefore complement existing systems and facilitate the characterization of
350 the biochemical regulation of gigaxonin and IF aggregation. Importantly, our cell
351 systems may also enable future high-throughput chemical or genetic screens to identify
352 candidate drugs and drug targets to ameliorate IF protein aggregation in GAN.

353

354 *Gigaxonin O-GlcNAc sites in human disease*

355 While our findings await investigation in other physiologically and clinically
356 relevant systems (e.g., rodent models, primary neuronal cultures, GAN patient cells),
357 our current results suggest novel hypotheses to test in GAN disease contexts. For
358 example, gigaxonin O-GlcNAcylation might be dysregulated in GAN patients, leading
359 to reduced gigaxonin stability or reduced interaction with, and ubiquitination of, IF
360 proteins and/or other recently discovered gigaxonin substrates involved in autophagy
361 (48) and sonic hedgehog signaling (70). While none of the nine identified candidate O-
362 GlcNAc sites is reported to be mutated in the GAN patients sequenced to date, it is still
363 possible that GAN disease allele mutations at other sites may affect O-GlcNAcylation
364 by inducing conformational changes that affect the access of OGT or OGA. More work
365 will be required to gain mechanistic insight into how O-GlcNAcylation regulates
366 gigaxonin function in GAN-relevant contexts. For instance, it will be important to
367 analyze the O-GlcNAcylation status of gigaxonin in human patients, which may be
368 helpful in predicting protein function *in vivo*.

369 *GAN*^{-/-} SH-SY5Y cells exhibit reduced proliferation and often grow as
370 individual cells, rather than clusters, suggesting that gigaxonin may play a role in
371 cancer-relevant phenotypes. To date, 276 different gigaxonin somatic mutations have

372 been identified in human tumor samples in the cBioportal database (71, 72). Among
373 these, two alter O-GlcNAc sites: An S272F mutation was identified in a cutaneous
374 melanoma and an S254C mutation in prostate adenocarcinoma. Our results predict that
375 the S272F mutation, at least, would impair gigaxonin function. IFs – especially
376 vimentin – participate in multiple cancer-relevant processes, including cell adhesion,
377 migration, the epithelial-to-mesenchymal transition and metastasis (73, 74). Therefore,
378 the biological significance of gigaxonin in cancer or other diseases may be
379 underappreciated, and the function of gigaxonin in tumor biology could be an
380 interesting subject of future work (75).

381

382 *Nutrient sensing and O-GlcNAcylation as potential modifiers of gigaxonin function and*
383 *GAN phenotypes*

384 Nutrient sensing is thought to be a prominent function of O-GlcNAcylation in
385 intracellular signaling (16, 19-24, 26, 27, 29). In a previous study, we reported that O-
386 GlcNAcylation of the KLHL protein KEAP1 varies dynamically with glucose levels
387 (14). Given these results, it is intriguing that gigaxonin O-GlcNAcylation also
388 fluctuates with metabolic cues (Figure 6). Together, these observations suggest that
389 nutrient status and IF proteostasis might be linked through the glycosylation of
390 gigaxonin in particular, and that O-GlcNAcylation may be a widespread regulatory
391 modification of KLHL proteins in general.

392 Here we show that deprivation of serum or glucose and glutamine (which feed the
393 HBP) reduces gigaxonin O-GlcNAcylation (Figure 6). Interestingly, serum starvation
394 was previously reported to potentiate IF aggregation in *GAN* loss-of-function cells, but
395 the underlying mechanism remained unclear (8). Recently, ATG16L-1, a key factor for
396 phagophore formation, was identified as a novel gigaxonin substrate (48), suggesting

397 another potential connection between nutrient starvation, autophagy and gigaxonin
398 function. In the future, it will be interesting to determine whether gigaxonin O-
399 GlcNAcylation impacts on ATG16L-1 and autophagy. We propose that nutrient or
400 growth factor starvation may trigger gigaxonin deglycosylation, reducing its interaction
401 with its substrates, such as vimentin or NF-L, and eventually leading to IF accumulation
402 and aggregation (Figure 7). However, serum starvation induces a variety of signaling
403 events that may directly or indirectly regulate OGT, OGA or UDP-GlcNAc availability,
404 including the glycosylation of IF proteins themselves. The influence of these factors on
405 the O-GlcNAcylation, regulation and function of gigaxonin will be a key focus of future
406 studies. In the longer term, it will be important to determine whether changes in
407 metabolic cues and gigaxonin glycosylation affect its function in vivo, and whether this
408 signaling is dysregulated in GAN patients, potentially contributing to the variability of
409 disease severity.

410

411 *Therapeutic implications*

412 Finally, although they must be further validated in clinically relevant models,
413 our findings may have important implications for GAN therapy. Currently, there are no
414 treatments to mitigate symptoms or disease progression, due partly to our imperfect
415 understanding of the molecular etiology of GAN. However, gene therapy approaches
416 have shown significant potential. For example, Gray and colleagues used engineered
417 adeno-associated virus (AAV) vectors to restore WT gigaxonin expression in *GAN*^{-/-}
418 mice and achieved persistent transgene expression in the central and peripheral nervous
419 systems for more than one year, accompanied by reduced neuronal IF protein
420 aggregation (76). More recently, the Gray lab conducted clinical trials of intrathecal
421 delivery of a scAAV9/JeT-GAN vector to re-express WT gigaxonin in GAN patients

422 (NCT02362438). Despite this clear promise, potential obstacles remain. For example,
423 endogenous gigaxonin is normally expressed at low levels and its ectopic
424 overexpression obliterates the entire IF network, leading to cell dysfunction (11, 12).
425 Therefore, improved knowledge of gigaxonin regulation – through O-GlcNAcylation
426 and other mechanisms – is needed to understand its activity in healthy neurons and,
427 perhaps, to tune its activity during GAN gene therapy (47, 77).

428

429 **Methods**

430

431 *Cell culture*

432 SH-SY5Y, HEK 293T, HeLa, and MDA-MB-231 were obtained from the Duke
433 Cell Culture Facility (CCF) and BJ5ta was obtained from American Type Culture
434 Collection (ATCC). Media used were: SH-SY5Y, DMEM/F-12 (Gibco #11320), with
435 HEPES (Gibco #15630); HeLa, 293T and MDA-MB-231, DMEM (Gibco #11995),
436 with HEPES; BJ5ta, 4:1 ratio DMEM (Gibco #11965) and Medium 199 (Gibco #11150).
437 All cell lines were maintained at 37 °C supplied with 5% CO₂ following standard
438 guidelines from the Duke CCF or ATCC and were cultured in medium supplied with
439 10% fetal bovine serum (FBS) and penicillin/streptomycin. For serum starvation, SH-
440 SY5Y cells were first washed twice with phosphate-buffered saline (PBS) and then
441 supplied with medium containing 10% or 0.1% FBS for 72 h (8). For glutamine
442 deprivation, HA-gigaxonin-transfected (24 h, total DNA: 10 µg per 10 cm plate) 293T
443 cells were first washed twice with PBS and then supplied medium (Gibco #A1443001;
444 10% dialyzed FBS, Sigma #F0392; glucose, #A2494001; sodium pyruvate, #11360070)
445 with or without L-glutamine (Gibco #25030081) for an additional 48 h before collecting
446 lysates.

447

448 *Preparation of gigaxonin-myc-6xHis protein*

449 Gigaxonin-myc-6xHis expression plasmid or control vector was transfected into
450 293T cells (15 cm plates x 6 for each condition). For transfection, each 15 cm plate was
451 transfected with 45 µl Mirus (TransIT-293 transfection reagent), 15 µg DNA (gigaxonin
452 or vector), and 750 µl Opti-MEM. After 41 h of transfection, 293T cells were treated
453 with 50 µM Thiamet-G and 4 mM glucosamine for additional 7 h. To collect lysates,
454 cells were washed by cold PBS twice, and harvested in 4 ml IP lysis buffer (0.1% SDS,
455 1% Triton X-100, 150 mM NaCl, 1mM EDTA, 20 mM Tris pH7.4) in the presence of
456 protease inhibitors and 5 µM PUGNAc. After measuring protein concentration by BCA
457 assay, an IP (25 mg protein at 2 mg/ml and 25 µg Myc antibody clone 9E10, Biolegend
458 #626801) was rotated at 4 °C overnight. The next day, 100 µl A/G beads slurry (pre-
459 washed by IP lysis buffer) was added into each sample and rotate at room temperature
460 (RT) for 2 h. After Myc-IP, the beads were then washed by 1 ml IP lysis buffer four
461 times, and the proteins were rotated and eluted by 300 µl buffer A (8 M urea, 300 mM
462 NaCl, 1%Triton X-100, and 5 mM imidazole) at RT for 15 min. Next, the eluted
463 proteins were incubated with Ni-NTA beads (100 µl slurry pre-equilibrated and washed
464 (three times) with buffer A for 2 h at RT. The Ni-NTA beads were then washed four
465 times with buffer A and proteins were eluted by 80 µl of elution buffer (8 M urea and
466 250 mM imidazole).

467

468 *Liquid chromatography-tandem mass spectrometry (LC-MS/MS) analysis of gigaxonin*
469 *O-GlcNAcylation*

470 Purified gigaxonin-myc-6xHis was separated by SDS-PAGE and Coomassie-
471 stained. Stained bands of the correct molecular weight were subjected to standard in-

472 gel trypsin digestion (https://genome.duke.edu/sites/genome.duke.edu/files/In-gelDigestionProtocolrevised_0.pdf). Extracted peptides were lyophilized to dryness
473 and resuspended in 12 μ l of 0.2% formic acid/2% acetonitrile. Each sample was
474 subjected to chromatographic separation on a Waters NanoAqity UPLC equipped with
475 a 1.7 μ m BEH130 C₁₈ 75 μ m I.D. X 250 mm reversed-phase column. The mobile phase
476 consisted of (A) 0.1% formic acid in water and (B) 0.1% formic acid in acetonitrile.
477 Following a 4 μ l injection, peptides were trapped for 3 minutes on a 5 μ m Symmetry
478 C₁₈ 180 μ m I.D. X 20 mm column at 5 μ l/minute in 99.9% A. The analytical column
479 was then switched in-line and a linear elution gradient of 5% B to 40% B was performed
480 over 60 minutes at 400 nL/minute. The analytical column was connected to a fused silica
481 PicoTip emitter (New Objective, Cambridge, MA) with a 10 μ m tip orifice and coupled
482 to a QExactive Plus mass spectrometer (Thermo) through an electrospray interface
483 operating in data-dependent acquisition mode. The instrument was set to acquire a
484 precursor MS scan from m/z 350-1800 every three seconds. In data-dependent mode,
485 MS/MS scans of the most abundant precursors were collected following higher-energy
486 collisional dissociation (HCD) fragmentation at an HCD collision energy of 27%.
487 Within the MS/MS spectra, if any diagnostic O-GlcNAc fragment ions (m/z 204.0867,
488 138.0545, or 366.1396) were observed, a second MS/MS spectrum of the precursor was
489 acquired with electron transfer dissociation (ETD)/HCD fragmentation using charge-
490 dependent ETD reaction times and either 30% or 15% supplemental collision energy
491 for $\geq 2+$ precursor charge states. For all experiments, a 60-second dynamic exclusion
492 was employed for previously fragmented precursor ions.

494 Raw LC-MS/MS data files were processed in Proteome Discoverer (Thermo
495 Scientific) and then submitted to independent Mascot searches (Matrix Science) against
496 a SwissProt database (human taxonomy) containing both forward and reverse entries

497 of each protein (20,322 forward entries). Search tolerances were 5 ppm for precursor
498 ions and 0.02 Da for product ions using semi-trypsin specificity with up to two missed
499 cleavages. Both y/b-type HCD and c/z-type ETD fragment ions were allowed for
500 interpreting all spectra. Carbamidomethylation (+57.0214 Da on C) was set as a fixed
501 modification, whereas oxidation (+15.9949 Da on M) and O-GlcNAc (+203.0794 Da
502 on S/T) were considered dynamic mass modifications. All searched spectra were
503 imported into Scaffold (v4.3, Proteome Software) and scoring thresholds were set to
504 achieve a peptide FDR of 1% using the PeptideProphet algorithm. When satisfactory
505 ETD fragmentation was not obtained, HCD fragmentation was used to determine O-
506 GlcNAc residue modification, using the number of HexNAcs identified in combination
507 with the number of serines and threonines in the peptide.

508 The mass spectrometry proteomics data have been deposited to the
509 ProteomeXchange Consortium (78) via the PRIDE (79) partner repository with the
510 dataset identifier PXD012488.

511

512 *CRISPR, quantitative PCR (qPCR) and shRNA*

513 To generate *GAN* knockout models, the lentiviral CRISPR/Cas9 system
514 developed by the Zhang lab was used (Addgene #52961) (80). Three different guide
515 RNAs (gRNAs) targeting the human *GAN* gene were selected using the CHOPCHOP
516 website (<http://chopchop.cbu.uib.no>) (gRNA1: GCAGAAGAACATCCTGGCGG,
517 gRNA2: GGTGCAGAAGAACATCCTGG, gRNA3:
518 CGGCCAGCCGTACATCAGG). SH-SY5Y and BJ5ta cells were infected with
519 gRNA/Cas9-expressing lentivirus and selected with puromycin to generate *GAN*-
520 deficient cell lines. The expression of gigaxonin and Cas9 was validated by Western
521 blotting after puromycin selection. *GAN*^{-/-} cell lines were maintained in puromycin-

522 containing media. To evaluate *GAN* mRNA levels, *GAN*^{-/-} or parental SH-SY5Y cells
523 were lysed to collect RNAs by RNeasy kit (Qiagen). *GAN* cDNAs from each group
524 were made by reverse transcriptase II (ThermoFisher) and quantified by qPCR. The
525 qPCR primer pairs were designed to target different region of *GAN* mRNA (168-F: 5'-
526 CCCGGTGCAGAAGAACATCC; 168-R: 5'-AGCCTGATCTGCCACTGAA; 180-
527 F: 5'-CCAGCCCCGTACATCAGGACA
528 180-R: 5'-GGTCAGCTGCCTGAACAAACA). The relative level of *GAN* mRNA was
529 normalized to β-actin mRNA in each group.

530 To knock down *GAN* expression, a lentiviral shRNA system was purchased
531 from Sigma (TRCN0000083858), targeting the *GAN* 3' UTR, with shRNA
532 CCGGCCACATAATATGGGATGCAATCTCGAGATTGCATCCCATATTATGTGGT
533 TTTTG.

534

535 *Immunofluorescence assay (IFA)*

536 To visualize IFs, control or *GAN*^{-/-} cells were seeded onto chamber slides (Thermo)
537 and transfected using Lipofectamine 3000 (Invitrogen) for 72 h. Cells were fixed in 4%
538 formaldehyde for 10 minutes, followed by three washes with 1X PBS, blocking at room
539 temperature for 1 h (5% bovine serum albumin in 1X PBS, 0.3% Triton X-100), and
540 incubation with anti-vimentin (Cell Signaling #5741, 1:200 in blocking solution) or
541 anti-HA (Santa Cruz #sc-7392, 1:100 in blocking solution) antibody at 4 °C overnight.
542 Nuclei were marked by DAPI (ThermoFisher #S36938) and F-actin was visualized by
543 phalloidin staining (Alexa Fluor 594 phalloidin #A12381), if applied. The above
544 staining protocol was also applied for NEFL (Cell Signaling #2837, 1:100), GM130
545 (Cell Signaling #12480, 1:100) and the V5 epitope tag (Cell Signaling #13202, 1:100).

546 All images were acquired on a Zeiss 780 inverted confocal microscope at the Duke
547 Light Microscopy Core Facility.

548 To visualize gigaxonin and vimentin in the HeLa Vimentin^{-/-} background,
549 200,000 HeLa Vimentin^{-/-} cells (55) were seeded in 6-well plates with a 22-mm
550 coverslip at the bottom of each well. 18 µL of TransIT-LT1 Transfection Reagent
551 (Mirus) was added to 250 µL of Opti-MEM I (Life Technologies), vortexed briefly,
552 and incubated at room temperature (RT) for 15 min. Then, 3 µg of one DNA from list
553 1 and list 2 (i.e. 6 µg of DNA in total) was added to the mixture. List 1: pLenti6 Neo
554 (negative control), EGFP-WT-vimentin, or EGFP-S49A-vimentin. List 2: pcDNA3
555 (negative control), HA-WT-gigaxonin, HA-S272A-gigaxonin, or HA-T277A-
556 gigaxonin. DNA mixtures were vortexed briefly and incubated at RT for 15 min before
557 transfection.

558 72 hours after transfection, cells were washed twice with 37 °C PBS, fixed with
559 4% paraformaldehyde (Sigma) gently on a shaker at RT for 20 min, permeabilized with
560 0.1% Triton X-100 (in PBS) with gentle shaking for 10 min and incubated in blocking
561 buffer (1% BSA in PBS) with rotation at RT for at least 30 min. Coverslips were co-
562 incubated with vimentin (D21H3, Cell Signaling, 1:100) and HA (F-7, sc-7392, Santa
563 Cruz Biotechnology, 1:100) antibodies at 4 °C overnight. Cells were washed three times
564 with PBS and co-incubated with a goat anti-mouse (H + L) Alexa Fluor 594- (Thermo
565 Fisher Scientific, A-11005, 1:200) and a goat anti-Rabbit (H + L) Alexa Fluor 488-
566 conjugated secondary antibody (Thermo Fisher Scientific, A-11008, 1:200) at RT for 1
567 h in the dark. Coverslips were washed with PBS three times and mounted
568 in ProLong Diamond anti-fade mounting medium with DAPI (Invitrogen, P36931) on
569 cover slides. Images were acquired using a sequential scan (multitrack) using a band-
570 pass emission filter at 410-484 nm for DAPI, 489-561 nm for vimentin, and 585-733

571 nm for HA on a Zeiss LSM 780 confocal laser scanning microscope fitted with an
572 oil Plan-Apochromat 40X/1.4 numerical aperture objective lens.

573 Gigaxonin-transfected cells were defined by setting a pre-determined HA signal
574 brightness threshold using the Fiji ImageJ particle analysis plugin. Vimentin
575 fluorescent intensity from a total of 80-100 cells with HA-positive signal was measured,
576 normalized to the HA-positive cell number, and averaged across various fields on each
577 cover glass. The mean values between the experimental groups from three biological
578 replicates were compared using Student's t-tests. Error bars representing the standard
579 error were included in the bar graph. $p < 0.05$ was considered statistically significant.

580 *Western blot (WB) and immunoprecipitation (IP)*

581 To measure vimentin levels after genetic or chemical manipulation, cells were
582 lysed in radioimmunoprecipitation assay (RIPA) buffer (ThermoFisher; 25 mM Tris-
583 HCl pH 7.6, 150 mM NaCl, 1% NP-40, 1% sodium deoxycholate, 0.1% SDS). Whole-
584 cell lysates were sonicated (>20 pulses) on ice until all insoluble material was dissolved.
585 Protein concentrations were determined by BCA assay and used to normalize all
586 samples. After boiling in sample buffer, the lysates were analyzed by WB. For most co-
587 IP experiments, cells were lysed in Pierce IP buffer (1% Triton X-100, 150 mM NaCl,
588 1 mM EDTA, and 25 mM Tris-HCl pH 7.5) supplemented with protease and
589 phosphatase inhibitors. 250 μ g to 500 μ g (final volume: 250 μ l; 1 to 2 μ g/ μ l) protein
590 lysates were used for IPs. For co-IP of EGFP-vimentin and HA-gigaxonin, cells were
591 transfected with the indicated constructs (total DNA: 10 μ g per 10 cm plate) for 24 h
592 and lysed in Pierce IP buffer. Lysates were sonicated gently (15 pulses) to disrupt
593 aggregates and spun down at 4 °C to collect the soluble fraction. 500 μ g of soluble
594 protein extract was incubated with HA or GFP antibody for 6 h before addition of

595 Dynabeads (ThermoFisher) for an overnight incubation at 4 °C. Beads were washed
596 four to five times with Pierce IP buffer. After washing, samples were eluted in 2X
597 sample buffer at 95 °C for 5 minutes. Antibodies used include CUL3 (Bethyl #A301-
598 109A), O-GlcNAc (Santa Cruz RL2, #sc-59624s; ThermoFisher 18B10.C7, #MA1-
599 038), β-tubulin (Cell Signaling #2128), Flag (Sigma #F1840), MYC (Santa Cruz #sc-
600 40), HA (Santa Cruz #sc-7392), ubiquitin (Santa Cruz #sc-8017), gigaxonin (Sigma
601 #SAB4200104), NEFL (Cell Signaling #2837), vimentin (Cell Signaling #5741),
602 vinculin (Santa Cruz #sc-73614), GAPDH (Santa Cruz #sc-25778), and GFP (Santa
603 Cruz #sc-8334).

604

605 *Statistical analysis*

606 For Figures 3D, S3D, 5C, and 5D, quantitative data were initially analyzed by one-
607 way ANOVA to minimize the probability of type I errors that might otherwise occur
608 from multiple tests performed on the same data set. The independent variables for the
609 ANOVA were either genotype (pcDNA3, WT-, S272A-, or T277A-gigaxonin) or a ratio
610 of genotypes (vimentin: WT-, S272A-, or T277A-gigaxonin, or WT-, S272A-, or
611 T277A-gigaxonin:vimentin), and the dependent variables were either fluorescent
612 intensity or relative binding efficiency. Following ANOVA, a Tukey's HSD post-hoc
613 test was performed on the data because sample sizes were equal between groups, and
614 in order to utilize a multiple comparison adjustment in calculating *p*-values.
615 Significance was assumed at *p* < 0.05. Both the ANOVAs and Tukey's HSD post-hoc
616 tests were calculated using JMP (Version 14.0. SAS Institute Inc., Cary, NC, 1989-
617 2019). For Figure 6C, Student's t-test (two tailed) was used to obtain the *p* value. *P* <
618 0.05 was considered significant.

619

620 **Study approval**

621 The study approval was not required because no animal or human specimens were
622 used in this study.

623

624 **Author contributions**

625 PHC, JH, JW, DTH, TJS, SP, BJB, AS, and AL performed the experiments. BMC
626 performed the statistical analysis and provided technical support for imaging analysis.
627 PHC, JTC, and MB designed the experiments and interpreted the results. PHC, JTC,
628 and MB wrote the manuscript. All authors reviewed and approved the manuscript. JTC
629 and MB supervised all aspects of the work.

630

631 **Acknowledgements**

632 We thank the members of the Boyce and Chi labs for critical discussion and
633 technical support, especially Dr. Erik Soderblom and the Duke Proteomics and
634 Metabolomics Shared Resource for O-GlcNAc site-mapping analyses. This study was
635 supported by NIH grants 1R01NS111588-01A1 (to JTC and MB), 5R01GM118847 (to
636 MB), R01GM124062 (to JTC), DoD grants (W81XWH-17-1-0143, W81XWH-15-1-
637 0486, W81XWH-19-1-0842 to JTC), Duke Cancer Institute (DCI) pilot fund (to MB
638 and JTC) and by a gift from the Hannah's Hope Fund (to MB and JTC).

References

1. Gordon N. Giant axonal neuropathy. *Dev Med Child Neurol.* 2004;46(10):717-9.
2. Bomont P, Cavalier L, Blondeau F, Ben Hamida C, Belal S, Tazir M, et al. The gene encoding gigaxonin, a new member of the cytoskeletal BTB/kelch repeat family, is mutated in giant axonal neuropathy. *Nat Genet.* 2000;26(3):370-4.
3. Berg BO, Rosenberg SH, and Asbury AK. Giant axonal neuropathy. *Pediatrics.* 1972;49(6):894-9.
4. Asbury AK, Gale MK, Cox SC, Baringer JR, and Berg BO. Giant axonal neuropathy--a unique case with segmental neurofilamentous masses. *Acta Neuropathol.* 1972;20(3):237-47.
5. Yang Y, Allen E, Ding J, and Wang W. Giant axonal neuropathy. *Cell Mol Life Sci.* 2007;64(5):601-9.
6. Dhanoa BS, Cogliati T, Satish AG, Bruford EA, and Friedman JS. Update on the Kelch-like (KLHL) gene family. *Hum Genomics.* 2013;7:13.
7. Furukawa M, He YJ, Borchers C, and Xiong Y. Targeting of protein ubiquitination by BTB-Cullin 3-Roc1 ubiquitin ligases. *Nat Cell Biol.* 2003;5(11):1001-7.
8. Bomont P, and Koenig M. Intermediate filament aggregation in fibroblasts of giant axonal neuropathy patients is aggravated in non dividing cells and by microtubule destabilization. *Hum Mol Genet.* 2003;12(8):813-22.
9. Boizot A, Talmat-Amar Y, Morrogh D, Kuntz NL, Halbert C, Chabrol B, et al. The instability of the BTB-KELCH protein Gigaxonin causes Giant Axonal Neuropathy and constitutes a new penetrant and specific diagnostic test. *Acta Neuropathol Commun.* 2014;2:47.
10. Lowery J, Jain N, Kuczmarski ER, Mahammad S, Goldman A, Gelfand VI, et al. Abnormal intermediate filament organization alters mitochondrial motility in giant axonal neuropathy fibroblasts. *Mol Biol Cell.* 2016;27(4):608-16.
11. Cleveland DW, Yamanaka K, and Bomont P. Gigaxonin controls vimentin organization through a tubulin chaperone-independent pathway. *Human Molecular Genetics.* 2009;18(8):1384-94.

12. Mahammad S, Murthy SN, Didonna A, Grin B, Israeli E, Perrot R, et al. Giant axonal neuropathy-associated gigaxonin mutations impair intermediate filament protein degradation. *J Clin Invest.* 2013;123(5):1964-75.
13. Israeli E, Dryanovski DI, Schumacker PT, Chandel NS, Singer JD, Julien JP, et al. Intermediate filament aggregates cause mitochondrial dysmotility and increase energy demands in giant axonal neuropathy. *Hum Mol Genet.* 2016;25(11):2143-57.
14. Chen PH, Smith TJ, Wu J, Siesser PF, Bisnett BJ, Khan F, et al. Glycosylation of KEAP1 links nutrient sensing to redox stress signaling. *EMBO J.* 2017;36(15):2233-50.
15. Hart GW, Slawson C, Ramirez-Correa G, and Lagerlof O. Cross talk between O-GlcNAcylation and phosphorylation: roles in signaling, transcription, and chronic disease. *Annual review of biochemistry.* 2011;80:825-58.
16. Hanover JA, Krause MW, and Love DC. The hexosamine signaling pathway: O-GlcNAc cycling in feast or famine. *Biochim Biophys Acta.* 2010;1800(2):80-95.
17. Hart GW. Three Decades of Research on O-GlcNAcylation - A Major Nutrient Sensor That Regulates Signaling, Transcription and Cellular Metabolism. *Front Endocrinol (Lausanne).* 2014;5:183.
18. Bond MR, and Hanover JA. A little sugar goes a long way: the cell biology of O-GlcNAc. *J Cell Biol.* 2015;208(7):869-80.
19. Hart GW, Housley MP, and Slawson C. Cycling of O-linked beta-N-acetylglucosamine on nucleocytoplasmic proteins. *Nature.* 2007;446(7139):1017-22.
20. Wells L, Vosseller K, and Hart GW. Glycosylation of nucleocytoplasmic proteins: signal transduction and O-GlcNAc. *Science.* 2001;291(5512):2376-8.
21. Love DC, and Hanover JA. The hexosamine signaling pathway: deciphering the "O-GlcNAc code". *Sci STKE.* 2005;2005(312):re13.
22. Bond MR, and Hanover JA. O-GlcNAc cycling: a link between metabolism and chronic disease. *Annu Rev Nutr.* 2013;33:205-29.
23. Mondoux MA, Love DC, Ghosh SK, Fukushige T, Bond M, Weerasinghe GR, et al. O-linked-N-acetylglucosamine cycling and insulin signaling are required for the glucose stress response in *Caenorhabditis elegans*. *Genetics.* 2011;188(2):369-82.

24. Kreppel LK, and Hart GW. Regulation of a cytosolic and nuclear O-GlcNAc transferase. Role of the tetratricopeptide repeats. *J Biol Chem.* 1999;274(45):32015-22.
25. Ruan H-B, Han X, Li M-D, Singh Jay P, Qian K, Azarhoush S, et al. O-GlcNAc Transferase/Host Cell Factor C1 Complex Regulates Gluconeogenesis by Modulating PGC-1 α Stability. *Cell Metabolism.* 2012;16:226-37.
26. Ruan HB, Dietrich MO, Liu ZW, Zimmer MR, Li MD, Singh JP, et al. O-GlcNAc transferase enables AgRP neurons to suppress browning of white fat. *Cell.* 2014;159(2):306-17.
27. Taylor RP, Geisler TS, Chambers JH, and McClain DA. Up-regulation of O-GlcNAc transferase with glucose deprivation in HepG2 cells is mediated by decreased hexosamine pathway flux. *J Biol Chem.* 2009;284(6):3425-32.
28. Taylor RP, Parker GJ, Hazel MW, Soesanto Y, Fuller W, Yazzie MJ, et al. Glucose deprivation stimulates O-GlcNAc modification of proteins through up-regulation of O-linked N-acetylglucosaminyltransferase. *J Biol Chem.* 2008;283(10):6050-7.
29. Liu K, Paterson AJ, Chin E, and Kudlow JE. Glucose stimulates protein modification by O-linked GlcNAc in pancreatic beta cells: linkage of O-linked GlcNAc to beta cell death. *Proc Natl Acad Sci U S A.* 2000;97(6):2820-5.
30. Cheung WD, and Hart GW. AMP-activated protein kinase and p38 MAPK activate O-GlcNAcylation of neuronal proteins during glucose deprivation. *J Biol Chem.* 2008;283(19):13009-20.
31. Shafi R, Iyer SP, Ellies LG, O'Donnell N, Marek KW, Chui D, et al. The O-GlcNAc transferase gene resides on the X chromosome and is essential for embryonic stem cell viability and mouse ontogeny. *Proc Natl Acad Sci U S A.* 2000;97(11):5735-9.
32. Keembiyehetty C, Love DC, Harwood KR, Gavrilova O, Comly ME, and Hanover JA. Conditional knockout reveals a requirement for O-GlcNAcase in metabolic homeostasis. *J Biol Chem.* 2015.
33. Yang YR, Song M, Lee H, Jeon Y, Choi EJ, Jang HJ, et al. O-GlcNAcase is essential for embryonic development and maintenance of genomic stability. *Aging cell.* 2012;11(3):439-48.

34. Wang P, and Hanover JA. Nutrient-driven O-GlcNAc cycling influences autophagic flux and neurodegenerative proteotoxicity. *Autophagy*. 2013;9(4):604-6.
35. Shin SH, Love DC, and Hanover JA. Elevated O-GlcNAc-dependent signaling through inducible mOGT expression selectively triggers apoptosis. *Amino Acids*. 2011;40(3):885-93.
36. Lazarus BD, Love DC, and Hanover JA. O-GlcNAc cycling: implications for neurodegenerative disorders. *Int J Biochem Cell Biol*. 2009;41(11):2134-46.
37. Hanover JA, and Wang P. O-GlcNAc cycling shows neuroprotective potential in C. elegans models of neurodegenerative disease. *Worm*. 2013;2(4):e27043.
38. Akan I, Olivier-Van Stichelen S, Bond MR, and Hanover JA. Nutrient-driven O-GlcNAc in proteostasis and neurodegeneration. *J Neurochem*. 2018;144(1):7-34.
39. Yuzwa SA, Shan X, Macauley MS, Clark T, Skorobogatko Y, Vosseller K, et al. Increasing O-GlcNAc slows neurodegeneration and stabilizes tau against aggregation. *Nat Chem Biol*. 2012;8(4):393-9.
40. Vaidyanathan K, Durning S, and Wells L. Functional O-GlcNAc modifications: implications in molecular regulation and pathophysiology. *Critical reviews in biochemistry and molecular biology*. 2014;49(2):140-63.
41. Yuzwa SA, and Vocadlo DJ. O-GlcNAc and neurodegeneration: biochemical mechanisms and potential roles in Alzheimer's disease and beyond. *Chemical Society reviews*. 2014;43(19):6839-58.
42. Zhu Y, Shan X, Yuzwa SA, and Vocadlo DJ. The emerging link between O-GlcNAc and Alzheimer disease. *J Biol Chem*. 2014;289(50):34472-81.
43. Chen PH, Chi JT, and Boyce M. KEAP1 has a sweet spot: A new connection between intracellular glycosylation and redox stress signaling in cancer cells. *Mol Cell Oncol*. 2017;4(6):e1361501.
44. Chen PH, Chi JT, and Boyce M. Functional crosstalk among oxidative stress and O-GlcNAc signaling pathways. *Glycobiology*. 2018;28(8):556-64.
45. Soomro A, Alsop RJ, Negishi A, Kreplak L, Fudge D, Kuczmarski ER, et al. Giant axonal neuropathy alters the structure of keratin intermediate filaments in human hair. *J R Soc Interface*. 2017;14(129).
46. Treiber-Held S, Budjarjo-Welim H, Reimann D, Richter J, Kretzschmar HA, and Hanefeld F. Giant axonal neuropathy: a generalized disorder of

- intermediate filaments with longitudinal grooves in the hair. *Neuropediatrics*. 1994;25(2):89-93.
47. Johnson-Kerner BL, Roth L, Greene JP, Wichterle H, and Sproule DM. Giant axonal neuropathy: An updated perspective on its pathology and pathogenesis. *Muscle Nerve*. 2014;50(4):467-76.
 48. Scrivo A, Codogno P, and Bomont P. Gigaxonin E3 ligase governs ATG16L1 turnover to control autophagosome production. *Nat Commun*. 2019;10(1):780.
 49. Johnson-Kerner BL, Garcia Diaz A, Ekins S, and Wichterle H. Kelch Domain of Gigaxonin Interacts with Intermediate Filament Proteins Affected in Giant Axonal Neuropathy. *PLoS One*. 2015;10(10):e0140157.
 50. Bomont P. Degradation of the Intermediate Filament Family by Gigaxonin. *Methods Enzymol*. 2016;569:215-31.
 51. Dequen F, Bomont P, Gowing G, Cleveland DW, and Julien JP. Modest loss of peripheral axons, muscle atrophy and formation of brain inclusions in mice with targeted deletion of gigaxonin exon 1. *J Neurochem*. 2008;107(1):253-64.
 52. Ganay T, Boizot A, Burrer R, Chauvin JP, and Bomont P. Sensory-motor deficits and neurofilament disorganization in gigaxonin-null mice. *Mol Neurodegener*. 2011;6:25.
 53. Armao D, Bailey RM, Bouldin TW, Kim Y, and Gray SJ. Autonomic nervous system involvement in the giant axonal neuropathy (GAN) KO mouse: implications for human disease. *Clin Auton Res*. 2016;26(4):307-13.
 54. Sanjana NE, Shalem O, and Zhang F. Improved vectors and genome-wide libraries for CRISPR screening. *Nat Methods*. 2014;11(8):783-4.
 55. Tarbet HJ, Dolat L, Smith TJ, Condon BM, O'Brien ET, 3rd, Valdivia RH, et al. Site-specific glycosylation regulates the form and function of the intermediate filament cytoskeleton. *Elife*. 2018;7.
 56. Shaw G, Morse S, Ararat M, and Graham FL. Preferential transformation of human neuronal cells by human adenoviruses and the origin of HEK 293 cells. *FASEB J*. 2002;16(8):869-71.
 57. Allen E, Ding J, Wang W, Pramanik S, Chou J, Yau V, et al. Gigaxonin-controlled degradation of MAP1B light chain is critical to neuronal survival. *Nature*. 2005;438(7065):224-8.

58. Wang W, Ding J, Allen E, Zhu P, Zhang L, Vogel H, et al. Gigaxonin interacts with tubulin folding cofactor B and controls its degradation through the ubiquitin-proteasome pathway. *Curr Biol*. 2005;15(22):2050-5.
59. Slawson C, Zachara NE, Vosseller K, Cheung WD, Lane MD, and Hart GW. Perturbations in O-linked beta-N-acetylglucosamine protein modification cause severe defects in mitotic progression and cytokinesis. *J Biol Chem*. 2005;280(38):32944-56.
60. Szklarczyk D, Morris JH, Cook H, Kuhn M, Wyder S, Simonovic M, et al. The STRING database in 2017: quality-controlled protein-protein association networks, made broadly accessible. *Nucleic Acids Res*. 2017;45(D1):D362-D8.
61. Zhang DD, Lo SC, Sun Z, Habib GM, Lieberman MW, and Hannink M. Ubiquitination of Keap1, a BTB-Kelch substrate adaptor protein for Cul3, targets Keap1 for degradation by a proteasome-independent pathway. *J Biol Chem*. 2005;280(34):30091-9.
62. Ridge KM, Shumaker D, Robert A, Hookway C, Gelfand VI, Janmey PA, et al. Methods for Determining the Cellular Functions of Vimentin Intermediate Filaments. *Methods Enzymol*. 2016;568:389-426.
63. Bond MR, and Hanover JA. O-GlcNAc Cycling: A Link Between Metabolism and Chronic Disease. *Annual Review of Nutrition*. 2013;33(1):205-29.
64. Zachara NE, and Hart GW. O-GlcNAc a sensor of cellular state: the role of nucleocytoplasmic glycosylation in modulating cellular function in response to nutrition and stress. *Biochim Biophys Acta*. 2004;1673(1-2):13-28.
65. Slawson C, Lakshmanan T, Knapp S, and Hart GW. A mitotic GlcNAcylation/phosphorylation signaling complex alters the posttranslational state of the cytoskeletal protein vimentin. *Mol Biol Cell*. 2008;19(10):4130-40.
66. Chou CF, and Omary MB. Mitotic arrest-associated enhancement of O-linked glycosylation and phosphorylation of human keratins 8 and 18. *J Biol Chem*. 1993;268(6):4465-72.
67. Haltiwanger RS, and Philipsberg GA. Mitotic arrest with nocodazole induces selective changes in the level of O-linked N-acetylglucosamine and accumulation of incompletely processed N-glycans on proteins from HT29 cells. *J Biol Chem*. 1997;272(13):8752-8.

68. Tang X, Keenan MM, Wu J, Lin CA, Dubois L, Thompson JW, et al. Comprehensive profiling of amino acid response uncovers unique methionine-deprived response dependent on intact creatine biosynthesis. *PLoS Genet.* 2015;11(4):e1005158.
69. Johnson-Kerner BL, Ahmad FS, Diaz AG, Greene JP, Gray SJ, Samulski RJ, et al. Intermediate filament protein accumulation in motor neurons derived from giant axonal neuropathy iPSCs rescued by restoration of gigaxonin. *Hum Mol Genet.* 2015;24(5):1420-31.
70. Arribat Y, Mysiak KS, Lescouzeres L, Boizot A, Ruiz M, Rossel M, et al. Sonic Hedgehog repression underlies gigaxonin mutation-induced motor deficits in giant axonal neuropathy. *J Clin Invest.* 2019.
71. Cerami E, Gao J, Dogrusoz U, Gross BE, Sumer SO, Aksoy BA, et al. The cBio cancer genomics portal: an open platform for exploring multidimensional cancer genomics data. *Cancer Discov.* 2012;2(5):401-4.
72. Gao J, Aksoy BA, Dogrusoz U, Dresdner G, Gross B, Sumer SO, et al. Integrative analysis of complex cancer genomics and clinical profiles using the cBioPortal. *Sci Signal.* 2013;6(269):pl1.
73. Richardson AM, Havel LS, Koyen AE, Konen JM, Shupe J, Wiles WG, et al. Vimentin Is Required for Lung Adenocarcinoma Metastasis via Heterotypic Tumor Cell–Cancer-Associated Fibroblast Interactions during Collective Invasion. *Clinical Cancer Research.* 2018;24(2):420-32.
74. Kidd ME, Shumaker DK, and Ridge KM. The role of vimentin intermediate filaments in the progression of lung cancer. *Am J Respir Cell Mol Biol.* 2014;50(1):1-6.
75. Kang JJ, Liu IY, Wang MB, and Srivatsan ES. A review of gigaxonin mutations in giant axonal neuropathy (GAN) and cancer. *Hum Genet.* 2016;135(7):675-84.
76. Bailey RM, Armao D, Nagabhushan Kalburgi S, and Gray SJ. Development of Intrathecal AAV9 Gene Therapy for Giant Axonal Neuropathy. *Mol Ther Methods Clin Dev.* 2018;9:160-71.
77. Mussche S, Devreese B, Nagabhushan Kalburgi S, Bachaboina L, Fox JC, Shih HJ, et al. Restoration of cytoskeleton homeostasis after gigaxonin gene transfer for giant axonal neuropathy. *Hum Gene Ther.* 2013;24(2):209-19.

78. Deutsch EW, Csordas A, Sun Z, Jarnuczak A, Perez-Riverol Y, Ternent T, et al. The ProteomeXchange consortium in 2017: supporting the cultural change in proteomics public data deposition. *Nucleic Acids Res.* 2017;45(D1):D1100-D6.
79. Perez-Riverol Y, Csordas A, Bai J, Bernal-Llinares M, Hewapathirana S, Kundu DJ, et al. The PRIDE database and related tools and resources in 2019: improving support for quantification data. *Nucleic Acids Res.* 2019;47(D1):D442-D50.
80. Sanjana NE, Shalem O, and Zhang F. Improved vectors and genome-wide libraries for CRISPR screening. *Nat Methods.* 2014;11(8):783-4.

Figure 1

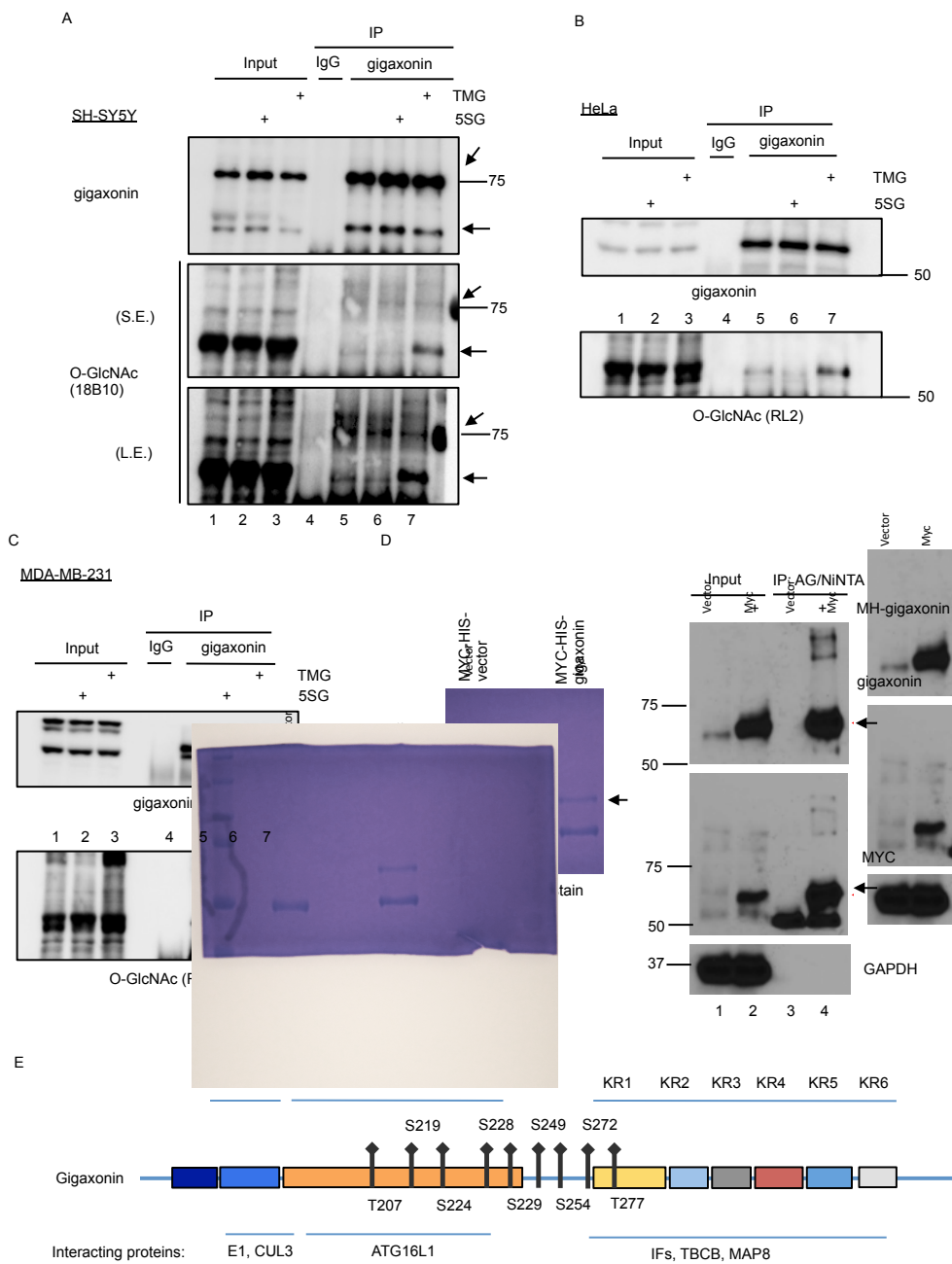
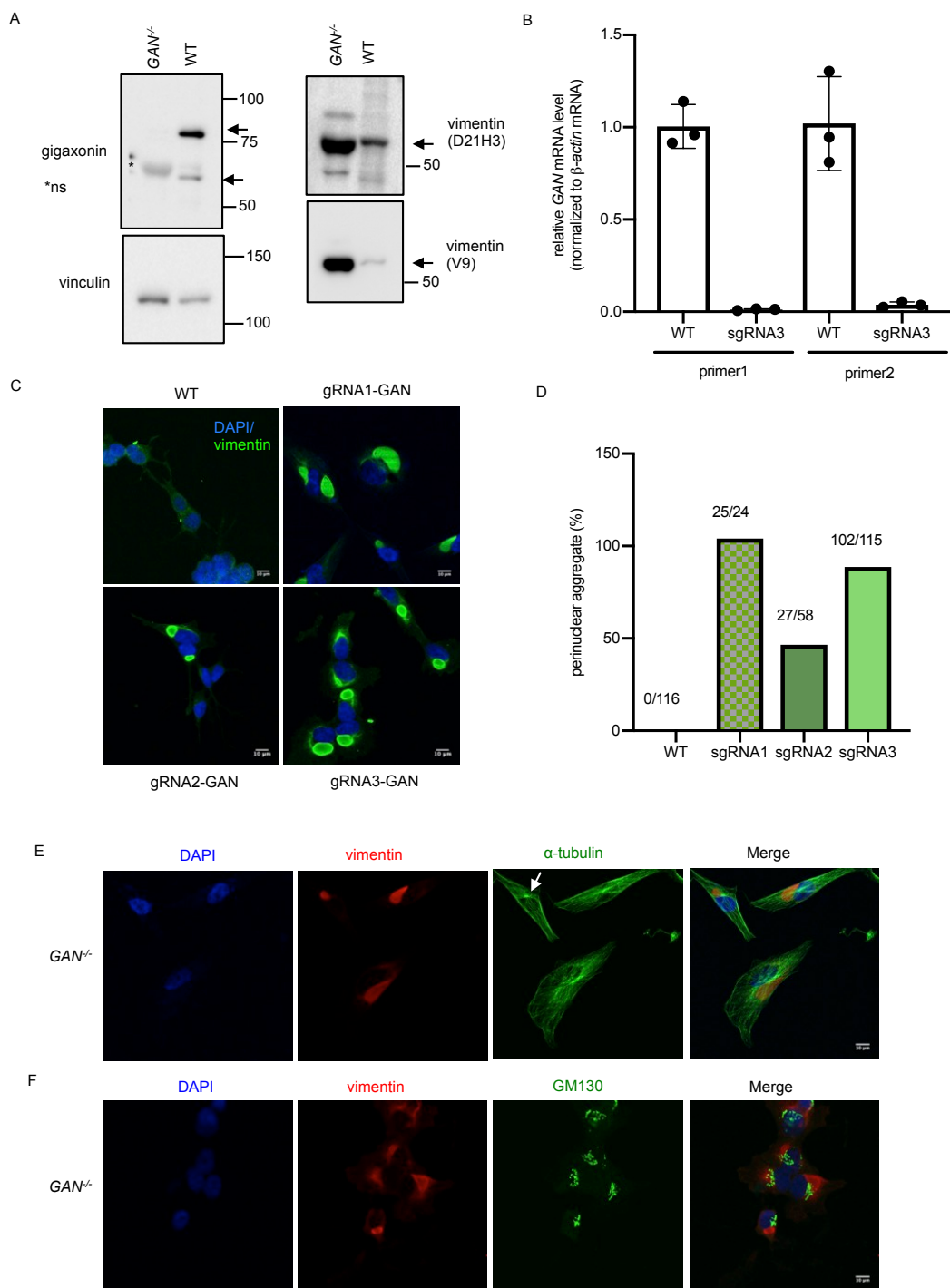


Figure 1. Site-specific O-GlcNAcylation of human gigaxonin

(A-C) Inhibition of OGT by 50 μ M Ac₄S₁GlcNAc (5SG) or of OGA by 25 μ M Thiamet-G (TMG) for 24 hours decreases or increases endogenous gigaxonin O-GlcNAcylation, respectively, in SH-SY5Y (S.E: short exposure; L.E.: long exposure),

HeLa (24 h), and MDA-MB-231 cells (34 h) (n=2). Cells were treated as indicated and endogenous gigaxonin was IPed from whole-cell lysates and analyzed by WB. Gigaxonin bands are indicated by arrows. (D) Coomassie blue stain (left) and WB (right) of myc-6xHis-gigaxonin protein tandem-purified from 293T cells for MS site-mapping (n=2). (E) MS analysis identified nine candidate O-GlcNAc sites on gigaxonin, indicated in the context of its domain structure and sites of interaction with known binding partners. Complete gigaxonin site-mapping data are available via ProteomeXchange (<http://www.proteomexchange.org>, dataset identifier PXD012488).

Figure 2



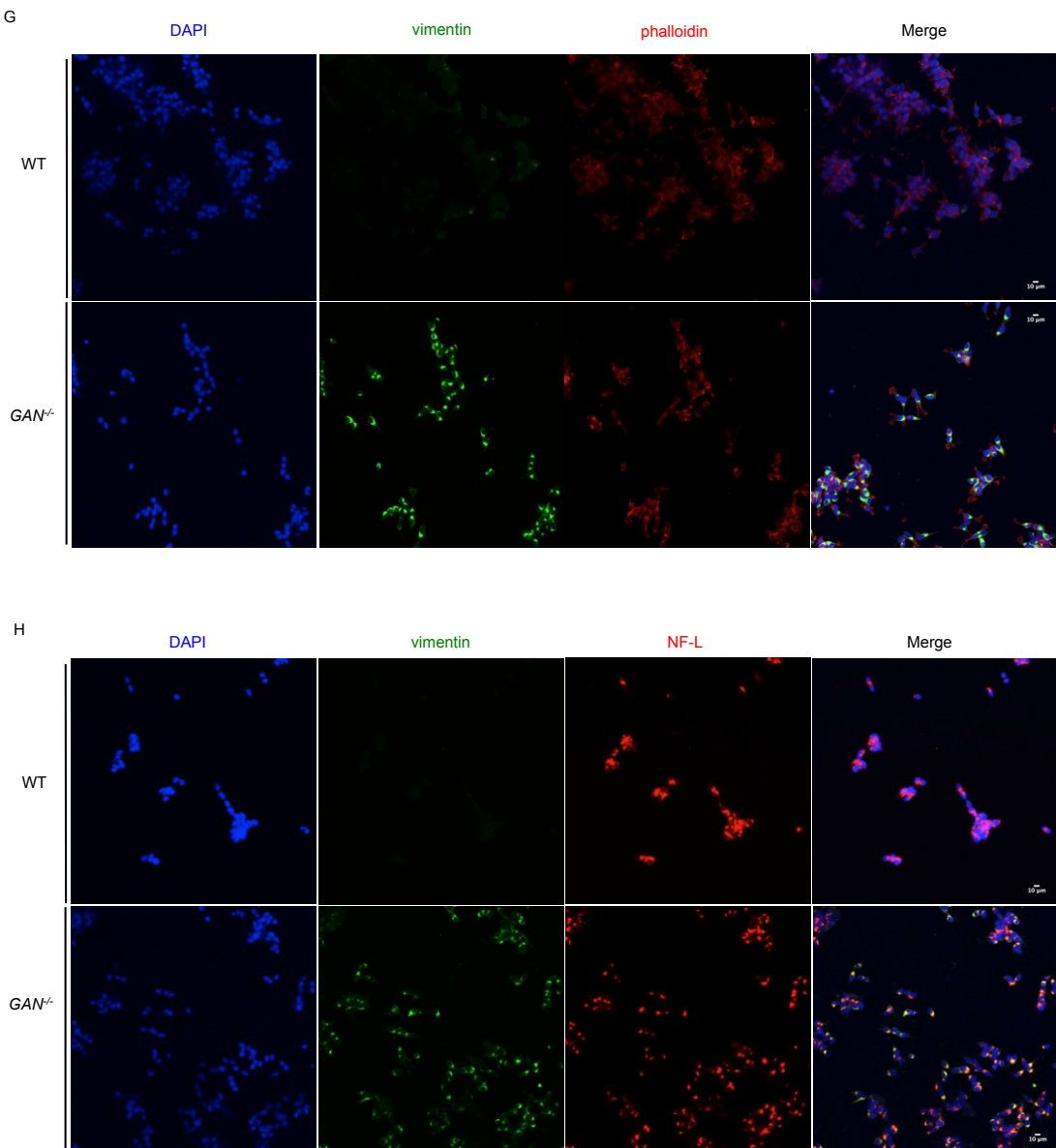


Figure 2. Generation of novel GAN model cell systems by CRISPR-Cas9 genome engineering

(A) SH-SY5Y cells were subjected to control or *GAN* gRNA genome editing. Lysates from single cell-derived clones were analyzed by WB, confirming loss of gigaxonin (arrow) and increased vimentin levels (arrows) in *GAN*^{-/-} cells, as compared to controls.

ns, non-specific. (B) Quantification of *GAN* mRNA expression in control and *GAN*^{-/-}

(gRNA) cells by qPCR (n=3; black dots represent individual biological replicates). (C)

Vimentin forms ovoid, perinuclear aggregates in *GAN*^{-/-} cells. Endogenous vimentin (green) and nuclei (DAPI, blue) were visualized by IFA in control and *GAN*^{-/-} cells derived from three independent gRNAs. (D) Quantification of ovoid and perinuclear aggregates in *GAN*^{-/-} cells. The number of ovoid aggregates and counted cells associated with each sgRNA is shown in the bar graph. (E) Vimentin aggregates co-localize with the microtubule organizing center in *GAN*^{-/-} cells, as detected by α-tubulin (white arrow) and vimentin IFA. (F) Vimentin aggregates do not co-localize with the Golgi marker GM130, as indicated by IFA in *GAN*^{-/-} cells. (G) F-actin distribution is not affected by gigaxonin loss, as indicated by IFA and phalloidin staining in *GAN*^{-/-} cells. (H) Co-localization of NF-L and vimentin in *GAN*^{-/-} cells, as indicated by IFA.

Figure 3

A

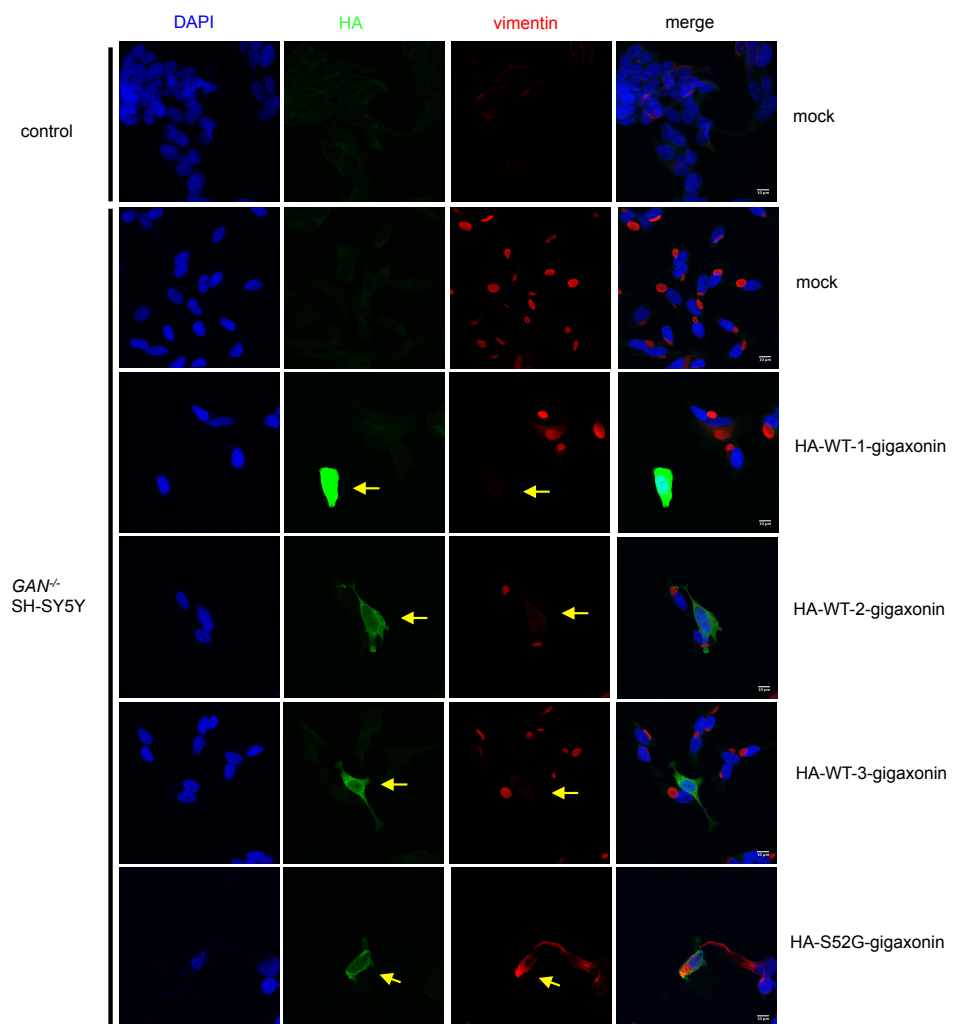


Figure 3

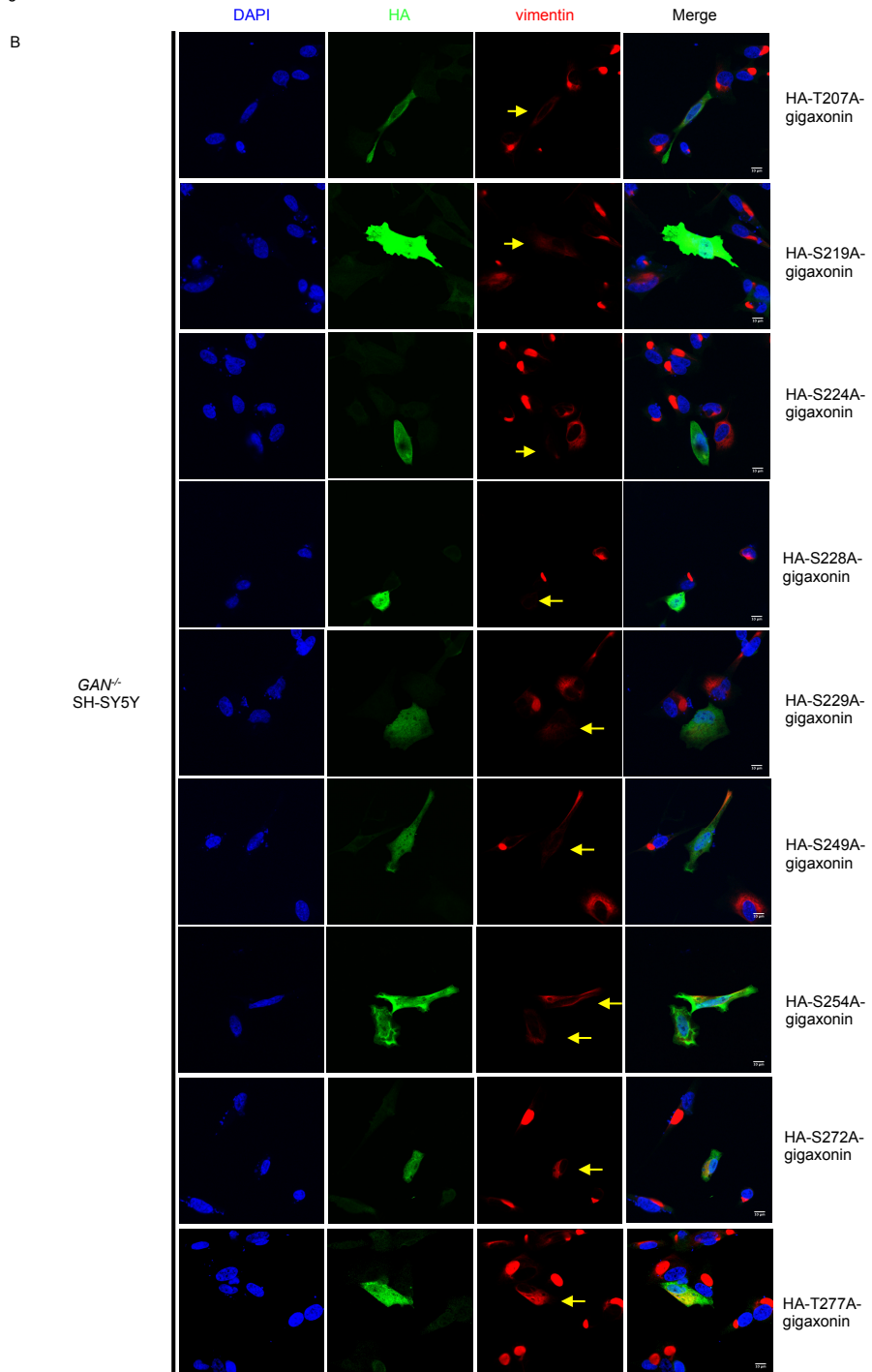


Figure 3

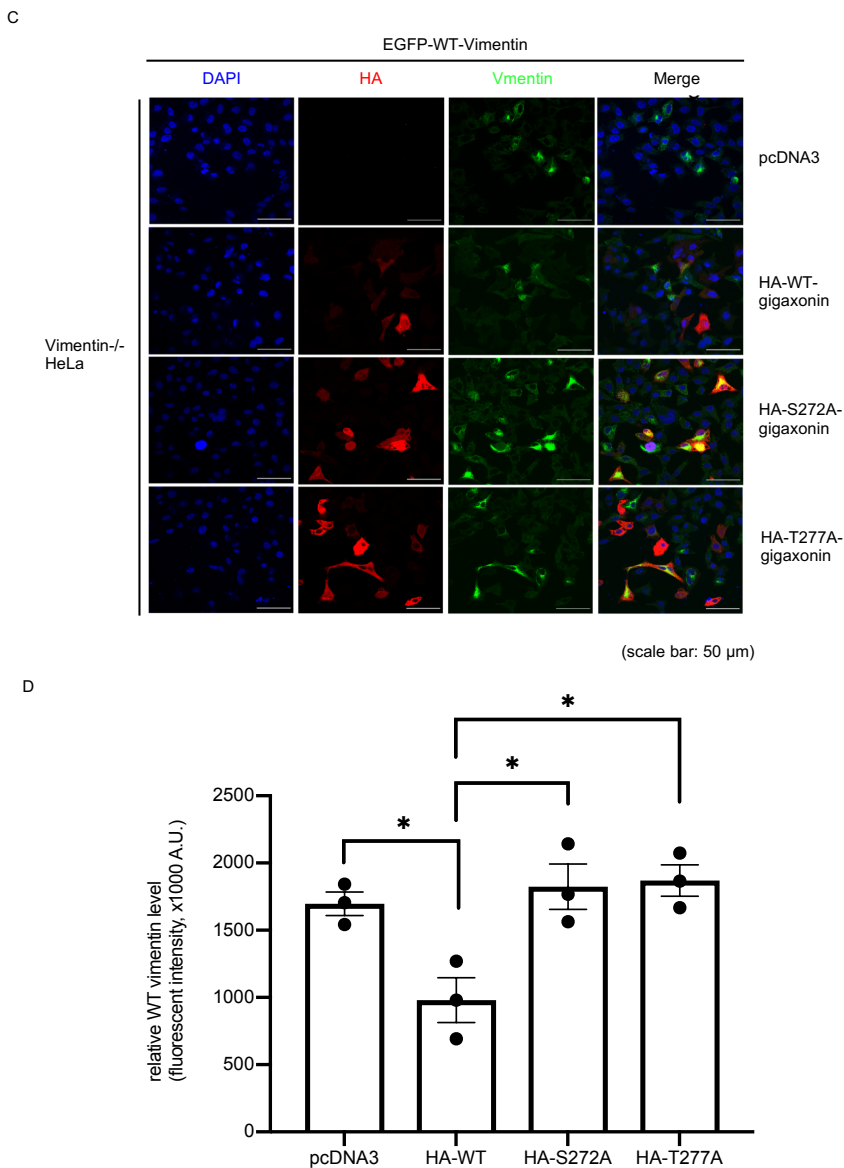


Figure 3. Unglycosylatable S272A and T277A gigaxonin mutants are impaired in clearing vimentin aggregates

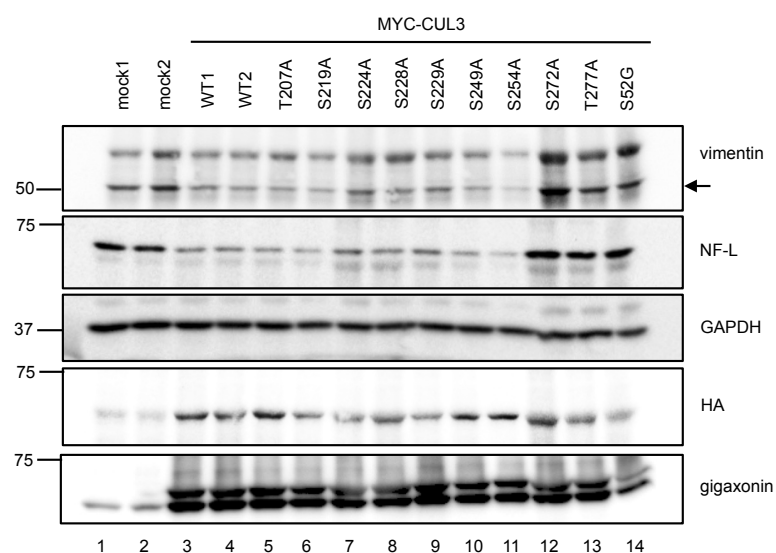
(A) Expression of WT gigaxonin, but not the S52G mutant, clears vimentin aggregates in *GAN*^{-/-} cells. Control (top row) or *GAN*^{-/-} (rows 2-6) SH-SY5Y cells were mock-transfected or transfected with HA-WT or HA-S52G gigaxonin constructs for 72 h. Expressed gigaxonin (HA, green) and endogenous vimentin (red) were visualized by IFA. Arrows indicate cells with aggregated vimentin (n=3). (B) *GAN*^{-/-} SH-SY5Y cells were transfected with the indicated HA-tagged unglycosylatable gigaxonin point-mutant constructs for 72 h. Expressed gigaxonin (HA, green) and endogenous vimentin (red) were visualized by IFA. Arrows indicate cells with aggregated vimentin (n=3).

(C) Vimentin^{-/-} HeLa cells were transfected with the indicated HA-tagged WT or unglycosylatable gigaxonin point-mutant constructs for 72 h. Expressed gigaxonin (HA, red) and endogenous vimentin (green) were visualized by IFA. Compared to WT, S272A and T277A gigaxonin exhibit reduced ability to clear EGFP-WT-vimentin. (D) Quantification of vimentin in gigaxonin-transfected cells in Fig. 3C. Vimentin fluorescence intensity from 80-100 HA-positive cells (or EGFP-positive cells in pcDNA3 group) was measured, normalized to the HA-positive cell number, and averaged across various fields on each cover glass. The mean values of the experimental groups from three biological replicates were analyzed first by one-way

ANOVA and then using Tukey's HSD post-hoc test. Error bars represent standard error and p -values < 0.05 were considered statistically significant.

Figure 4

A



B

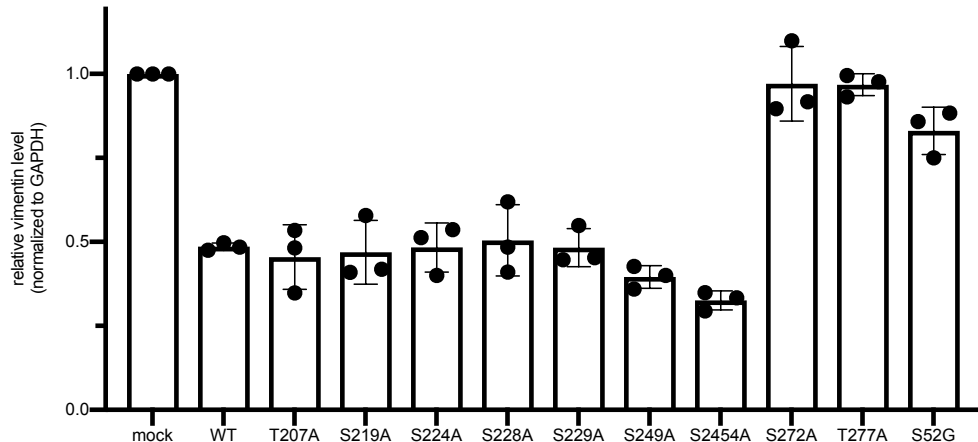


Figure 4. Unglycosylatable S272A and T277A gigaxonin mutants are impaired in cooperating with CUL3 to reduce IF protein levels

(A) 293T cells were mock-transfected or transfected with MYC-CUL3 and WT or point-mutant HA-gigaxonin constructs, as indicated, for 72 h. Cell lysates were

analyzed by WB. (B) Quantification of vimentin protein level (normalized to GAPDH level) in mock-, WT-, or indicated point-mutant gigaxonin-transfected cells in Fig. 4A (n=3; black dots represent individual biological replicates, mean ± standard deviation).

Figure 5

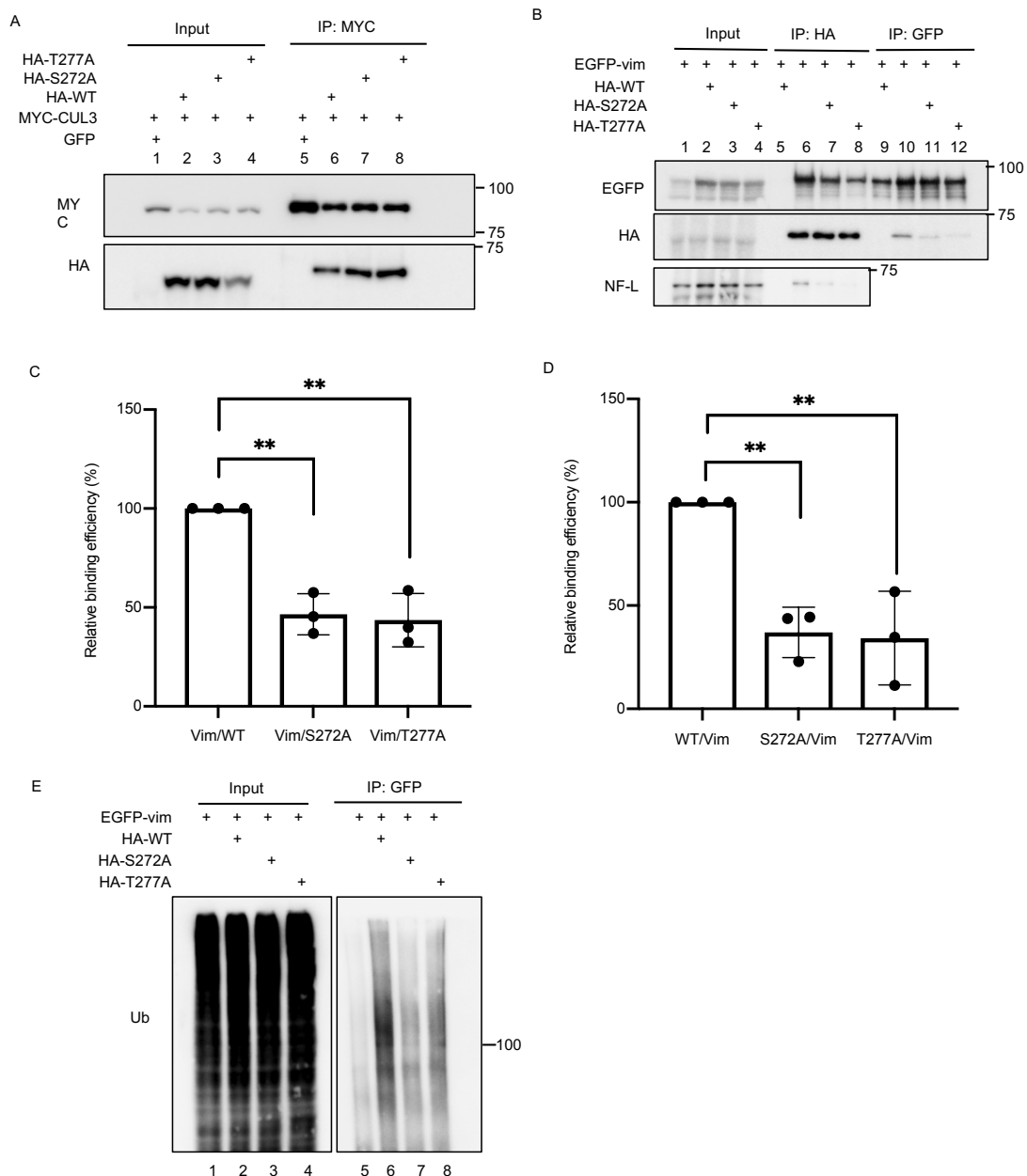


Figure 5. S272A and T277A gigaxonin mutants have reduced interaction with vimentin and NF-L

(A) 293T cells were co-transfected with constructs encoding GFP or WT, S272A or T277A HA-gigaxonin and MYC-CUL3, as indicated, for 46 h. Lysates were subjected to MYC IP and analyzed by WB. The interaction between S272A or T277A gigaxonin with CUL3 is not reduced, relative to WT (n=2). (B) 293T cells were co-transfected with constructs encoding WT, S272A or T277A HA-gigaxonin and EGFP-vimentin, as indicated, for 30 h. Lysates were subjected to HA or GFP IP and analyzed by WB. The S272A and T277A gigaxonin mutants show reduced interaction with vimentin and NF-L. (C, D) Quantification of the relative binding efficiency between vimentin and indicated gigaxonin variants from IP-WB in Fig. 5B. The vimentin/WT-gigaxonin interaction was normalized to 100%. (n=3; black dots represent individual biological replicates). The mean values from the three replicates were analyzed first by one-way ANOVA and then using Tukey's HSD post-hoc test. Error bars represent standard deviation and p -values < 0.05 were considered statistically significant, ** $p < 0.01$. (E) 293T cells were co-transfected with constructs encoding EGFP-vimentin and WT, S272A or T277A HA-gigaxonin, as indicated, for 30 h. Lysates were subjected to GFP IP and analyzed by ubiquitin (Ub) WB. Polyubiquitination of vimentin is reduced in S272A or T277A gigaxonin-expressing cells, compared to WT (n=3).

Figure 6

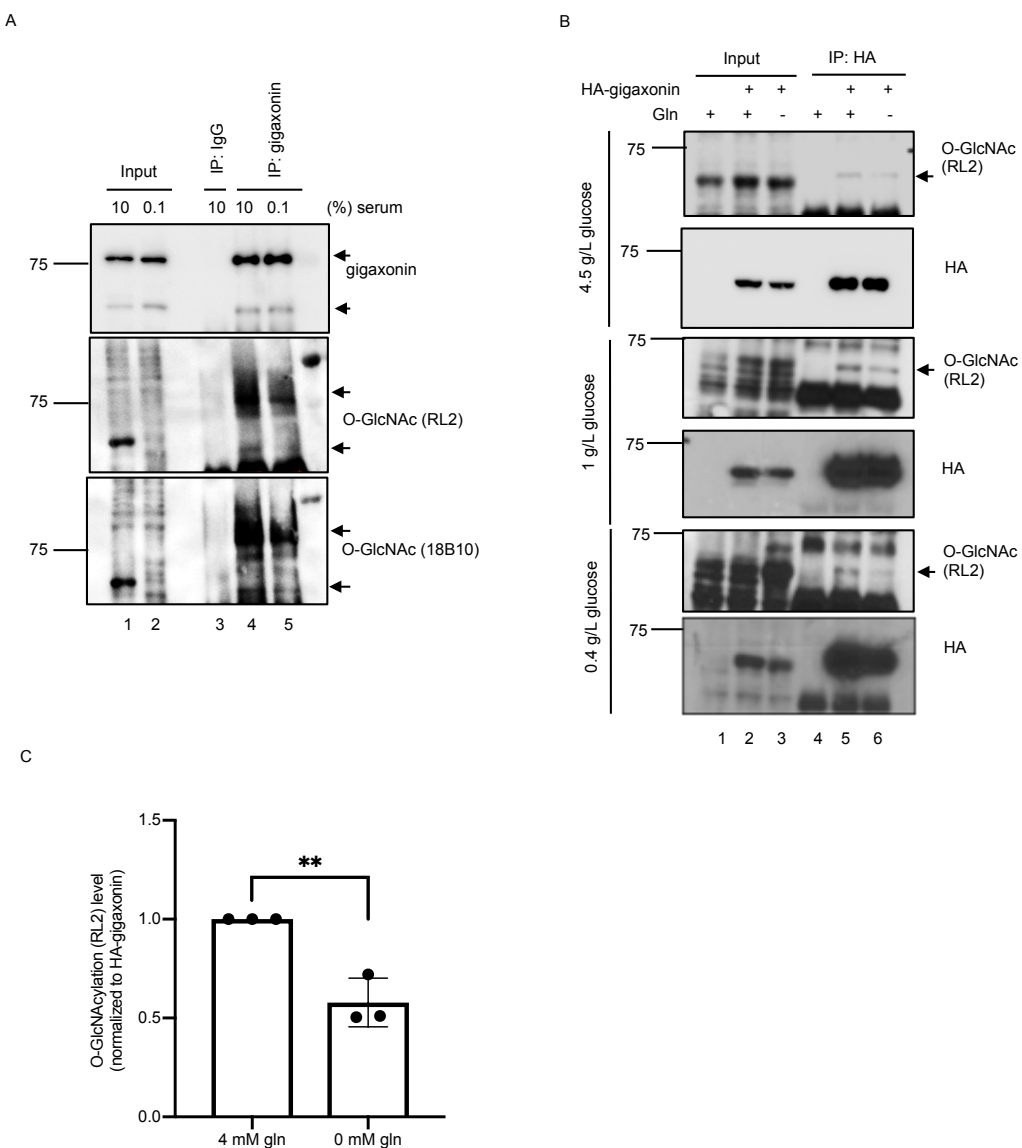


Figure 6. Nutrient-sensitive regulation of gigaxonin O-GlcNAcylation

(A) SH-SY5Y cells were treated with 10% or 0.1% serum for 72 h, as indicated, and lysed. Endogenous gigaxonin was IP-ed and analyzed by WB. Gigaxonin O-GlcNAcylation is reduced after serum starvation, as indicated by two different anti-O-GlcNAc monoclonal antibodies (representative results from three biological replicates).

Arrows indicate gigaxonin bands. (B) 293T cells were transfected with WT HA-

gigaxonin for 24 h, treated with control (4 mM) or glutamine-free medium for an additional 48 h under various glucose concentration, as indicated, and then lysed. HA-gigaxonin was IP-ed and analyzed by WB. Gigaxonin O-GlcNAcylation is reduced after glutamine starvation under low glucose condition, as indicated by anti-O-GlcNAc (RL-2) WB. Arrows indicate gigaxonin bands. (C) Quantification of gigaxonin glycosylation under glutamine starvation and low glucose condition (0.4 g/L) in Fig. 6B (n=3; black dots represent individual biological replicates, mean \pm standard deviation, Student's t-tests, ** $p < 0.01$).

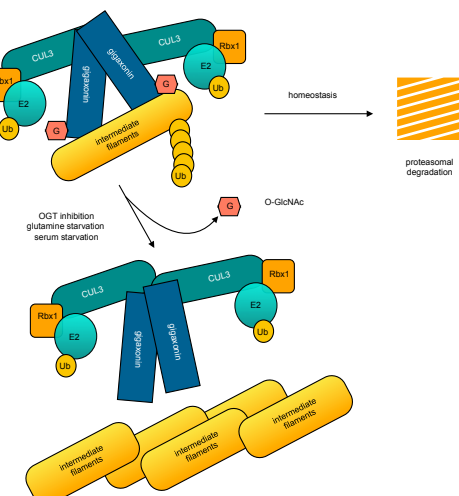


Figure 7. Proposed model for O-GlcNAc-mediated regulation of gigaxonin

Taken together, our results suggest that O-GlcNAcylation of gigaxonin promotes its optimal interaction with IF proteins (e.g., vimentin or NF-L) to facilitate their polyubiquitination and proteasome-mediated degradation. Nutrient deprivation and/or other stimuli lead to reduced gigaxonin O-GlcNAcylation, especially at S272 and T277, inhibiting its interaction with IFs and leading to their accumulation.